Calculating Geochemical Reaction Pathways - Exploration of the Inner-Sphere Water Exchange Mechanism in $Al(H_2O)_6^{3+}(aq) + nH_2O$ with ab Initio Calculations and Molecular Dynamics

R. James Evans,*,† James R. Rustad,† and William H. Casey†,‡

Department of Geology and Department of Chemistry, University of California, One Shields Avenue, Davis, California 95616

Received: December 12, 2007; In Final Form: February 8, 2008

We have simulated exchange of inner-sphere and bulk water molecules for different sizes of $Al^{3+}(aq)$ clusters, $Al(H_2O)_6^{3+} + nH_2O$ for $n = 0$, 1, 6, or 12, with ab initio and molecular dynamics simulations, in order to understand how robust the ab initio method is for identifying hydrolytic reaction pathways of particular importance to geochemistry. In contrast to many interfacial reactions, this particular elementary reaction is particularly simple and well-constrained by experiment. Nevertheless, we find that a rich array of parallel reaction pathways depend sensitively on the details of the solvation sphere and structure and that larger clusters are not necessarily better. Inner-sphere water exchange in $Al^{3+}(aq)$ may occur through two Langford−Gray dissociative pathways, one in which the incoming and outgoing waters are cis, the other in which they are trans to one another. A large majority of exchanges in the molecular dynamics simulations occurred via the trans mechanism, in contrast to the predictions of the ab initio method. In $Al(H_2O)_6^{3+} + H_2O$, the cis mechanism has a transition state of 84.3 kJ/mol, which is in good agreement with previous experimental and ab initio results, while the trans mechanism has only a saddle point with two negative frequencies, not a transition state, at 89.7 kJ/mol. In addition to the exchange mechanisms, dissociation pathways could be identified that were considerably lower in energy than experiment and varied considerably between 60 and 100 kJ/mol, depending on the particular geometry and cluster size, with no clear relation between the two. Ab initio calculations using large clusters with full second coordination spheres ($n = 12$) were unable to find dissociation or exchange transition states because the network of hydrogen bonds in the second coordination sphere was too rigid to accommodate the outgoing inner-sphere water. Our results indicate that caution should surround ab initio simulation of complicated dynamic processes such as hydrolysis, ion exchange, and interfacial reactions that involve several steps. Dynamic methods of simulation need to accompany static methods such as ab initio calculation, and it is best to consider simulated pathways as hypotheses to be tested experimentally rather than definitive properties of the reaction.

1. Introduction

The influential paper by Gibbs[1] led geochemists to use quantum-mechanical models to interpret the pathways for difficult interfacial reactions.[2−14] The simulations correspond to single elementary reactions; that is, to individual bond-breaking or bond-forming events, often involving the movement of a few atoms only, with the formation of an unstable transition-state complex. The parameters extracted from the simulation are usually the structure of the transition-state complex(es) (e.g., the metals and their coordinating ligands) and the activation energy corresponding to a complicated overall reaction, which is used to identify the reaction pathway. Because these reactions are commonly impossible to probe experimentally, the appeal of the simulations to Earth scientists is strong.

Scientists in the mid-1990s began to attempt to estimate the reaction parameters and pathways for the simplest of aqueous reactions, exchange of a single inner-sphere water of hydration with a water molecule in the bulk solution[15−21] in recognition that some experimental verifications were needed. The attraction of ab initio simulation of transition states using clusters is profound; time is eliminated from the problem, and the properties can be identified from inexpensive static calculations, corresponding to 0 K.

In this paper we examine the exchange of a water molecule from around the Al^{3+} ion in aqueous solution using various approximations to the solvation shell. Our goal is a comprehensive examination of the dependence of the reaction structure and energies on details of the simulation, with the idea that similar dependencies will be present in the simulation of unseen surface reactions. We choose to simulate the $Al^{3+}(aq)$ ion because of the high quality of the experimental data and because of its interest to geochemists. Hugi-Cleary et al.[22] measured the rates and the activation parameters using both the ^{17}O NMR line-broadening method and by ^{17}O-injection. They report $k_{ex}^{298} = 1.29\ s^{-1}$, $\Delta H^{\ddagger} = 84.7$ kJ/mol, $\Delta S^{\ddagger} = 41.6$ J/mol·K, and $\Delta V^{\ddagger} = 5.7\ cm^3$/mol, consistent with a dissociative interchange (I_d) reaction mechanism (see also refs 23, 24).

The common meaning of the "mechanism" of water exchange reactions is the extent to which the first- and second-sphere waters move simultaneously in exchange, with the accompanying breaking and formation of bonds. In a pure dissociative (D) exchange, a water leaves the first coordination sphere (i.e., a

* Corresponding author. E-mail: rjamesevans@gmail.com.
† Department of Geology.
‡ Department of Chemistry.

10.1021/jp7116888 CCC: $40.75
Published on Web 03/27/2008

bond is broken) before a new water enters and the transition state has a reduced coordination number. In a pure associative (A) mechanism, the incoming water enters the first coordination sphere from the second (i.e., a bond is formed) before another water leaves, causing the coordination number to increase. For octahedral metals like Al^{3+}(aq), the incoming and outgoing steps occur with varying degrees of simultaneity to give associative interchange (I_a), interchange (I), or dissociative interchange (I_d) mechanisms. The I_d mechanism that is assigned to water exchange around Al^{3+} means that the reaction pathway involves concerted motions of the entering and leaving water molecules, and both bond-breaking and formation occurring together, with bond-breaking dominant.

In addition to this usual meaning of mechanism, we also consider the more specific details of how the first- and second-sphere waters move during the exchange, particularly when the first-sphere waters are not symmetry equivalent. This is the case in the commonly used method of representing the whole second sphere by just a few (or one) representative waters.[16−18,21,22] In such cases, there is likely to exist more than one pathway[39] of a given type (D, A, I, etc.), with different transition states and activation energies, where it is unclear which corresponds to the exchange mechanism in the presence of a full second sphere.

2. Simulation Details

Most reactions simulated were dissociation reactions where a water from the first coordination sphere of Al^{3+} is moved into the second coordination sphere, using the Al−O distance d(Al−O) as the reaction coordinate. Energy curves for the removal (or addition) of a first-sphere water were calculated by optimizing the structure of $Al(H_2O)_6^{3+} + nH_2O$, where n = 0, 1, 2, 6, or 12, with the desired Al−O distance frozen. Potential transition states were checked by performing a frequency calculation and searching for a negative frequency. All ab initio calculations were performed in the gas phase approximation using restricted Hartree−Fock (basis sets 6-31G(d) on all atoms) in *Gaussian 03*.[25] We have made no attempt to compensate for the effects of the surrounding solvent, beyond extending the cluster size. Gas-phase Hartree−Fock calculations have been shown to give reasonable geometries and energies for clusters in solution, for ions with +2 or +3 charge, and clusters with neutral ligands and small permanent dipole moment.[26−28] For computational speed, we have not included any polarization functions in the basis set, although they are recommended for second-row atoms;[26] however, our cluster geometries and energies compare well with the results of Wassermann et al.[29] for $Al(H_2O)_6^{3+}$ and Kowall et al.[18] for $Al(H_2O)_6^{3+} + H_2O$ at higher levels of theory. Reported energies do not include zero point corrections.

Molecular dynamics (MD) simulations were performed with *GROMACS*[30] using CLAYFF interatomic potentials.[31] The simulations were run with a constant temperature of 300 K and constant pressure of 1 bar.

2.1. Nomenclature. Like many metal cations, Al^{3+}(aq) has six water molecules in its first coordination sphere, organized in an octahedral geometry (Figure 1), for a cluster stoichiometry of $Al(H_2O)_6^{3+}$. In the absence of any second-sphere waters, the AlO_6 core has O_h symmetry, with an optimized Al−O bond length of 1.93 Å. The $Al(H_2O)_6^{3+}$ cluster as a whole has a modified octahedral symmetry with point group T_h.

We orient the undistorted $Al(H_2O)_6^{3+}$ cluster as in Figure 1, such that the octahedral axes lie along the coordinate axes and the waters whose oxygen atoms sit on the x axis lie in the xy plane. Let the oxygen atom sitting on the positive x axis be labeled O_x^+, the oxygen atom on the negative y axis O_y^-, and so forth. When applying a continuous distortion to the cluster, such as increasing one Al−O distance, the waters in the distorted cluster are identified with the corresponding waters in the undistorted cluster.

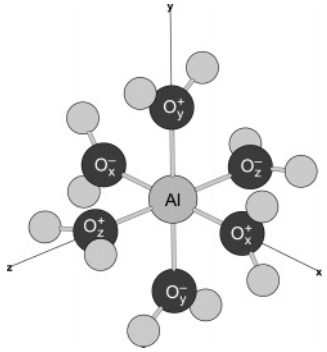

Figure 1. Undistorted aqueous cluster $Al(H_2O)_6^{3+}$, with labels on the first-sphere waters (see text).

3. Results and Discussion

Because Al^{3+} is predicted to have an I_d exchange mechanism, we began by dissociating a water ligand from bare gas-phase $Al(H_2O)_6^{3+}$. Next we added increasing numbers of spectator waters during the dissociation, exploring as many relevant pathways as possible, with the intent of obtaining an increasingly better approximation of the effects of higher coordination spheres on the dissociation. Finally, we switched from ab initio to molecular dynamics simulations with over 200 spectator waters and periodic boundary conditions, simulating Al^{3+} in bulk water.

3.1. Dissociation of a Water from Bare $Al(H_2O)_6^{3+}$. The first reaction relevant to water exchange in $Al(H_2O)_6^{3+}$, without involving second-sphere waters, is dissociation of $Al(H_2O)_6^{3+}$ in the gas phase. We remove a single water to produce a five-coordinated intermediate:

$$Al(H_2O)_6^{3+} \rightarrow Al(H_2O)_5^{3+} + H_2O \qquad (1)$$

The six waters are symmetry equivalent, so we arbitrarily remove the water labeled O_x^+. The energy of the cluster as a function of d(Al−O_x^+), relative to the undistorted cluster, is shown in Figure 2. A local maximum occurs at d(Al−O_x^+) = 3.04 Å, ΔE = 82.8 kJ/mol; a frequency calculation at this point shows a single negative frequency of −103.7 cm^{-1}, indicating a transition state. (The normal mode corresponding to this frequency is shown by the arrows in Figure 5A.) The local minimum at d(Al−O_x^+) = 3.41 Å, ΔE = 79.0 kJ/mol would correspond to a reaction intermediate in a purely dissociative exchange. The transition state (TS) and intermediate (Int.) structures are shown in the inset of Figure 2.

As the Al−O_x^+ distance increases, the O_z^+−Al−O_z^- angle decreases from 180° in the undistorted octahedron to 104° in the intermediate, as those protons on the O_z^+ and O_z^- waters pointing in the direction of the departing O_x^+ water are attracted by the O_x^+ oxygen. In the intermediate, which has a trigonal bipyramid structure with O_y^- and O_y^+ forming the pyramidal axis, the departing O_x^+ water has formed hydrogen bonds with the nearest protons of the O_z^+ and O_z^- waters. At Al−O_x^+ distances beyond the intermediate, the O_z^+−Al−O_z^- angle continues to decrease for a while as the Al−O_x^+ distance increases, until repulsion between the O_z^+ and O_z^- protons overcomes the attraction of the distant O_x^+ oxygen, and the angle

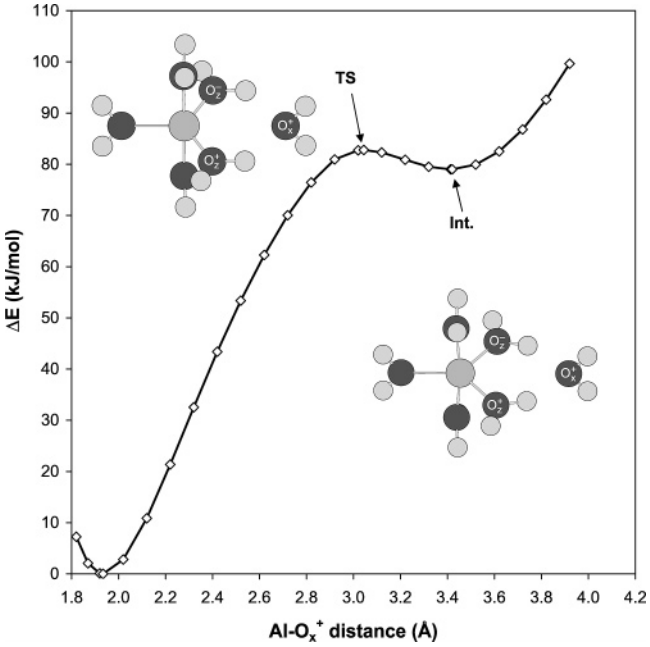

Figure 2. Energy profile for removing a first-sphere water (O_x^+) from $Al(H_2O)_6^{3+}$. Energies are relative to the starting cluster. The transition state (TS) and reaction intermediate (Int.) are labeled with structures shown in the inset.

begins to relax. In comparison, a bare $Al(H_2O)_5^{3+}$ cluster (i.e., with no second-sphere waters) has a square-pyramidal structure, with an $O_z^+-Al-O_z^-$ angle of 173°.

This dissociation process is the same as that described previously by Wassermann et al.[29] At a higher level of theory, they found a transition state of 96 kJ/mol at 3.0 Å and an intermediate of 79 kJ/mol at 3.5 Å.

3.2. $Al(H_2O)_6^{3+} + H_2O$ Cluster. *3.2.1. Structure.* Next, we examine how the geometries and energetics of this elementary reaction are affected by the addition of one water molecule, O_W, in the second coordination sphere. The water forms either one or two hydrogen bonds between its oxygen and protons(s) on the $Al(H_2O)_6^{3+}$ cluster. The single H-bonded structure, the hydrogen bond between O_W and O_x^+, is shown in Figure 3A. The structure is symmetric through reflection in the *xy* plane with point group C_s. The $Al-O_x^+$ bond shortens from 1.93 Å in bare $Al(H_2O)_6^{3+}$ to 1.87 Å, while the other first-sphere Al−O bonds lengthen to 1.94−1.95 Å. The $Al-O_W$ distance is 3.95 Å, and the H−O distance in the hydrogen bond is 1.54 Å.

Two double H-bonded structures, with O_W bonded to O_x^+ and O_y^+, with very similar energies are shown in parts B−E of Figure 3. The lowest in energy is a completely asymmetric structure (point group C_1), shown in Figure 3B and C, which is 4.4 kJ/mol lower in energy than the single H-bonded structure. The $H-O_W$ distances are 1.79 Å on water O_x^+ and 1.83 Å on O_y^+. The oxygen of the second-sphere water lies above the *xy* plane (i.e., with $z > 0$ in the coordinate system of Figure 1), and the $Al-O_W$ distance is 3.73 Å, significantly smaller than in the single H-bonded structure. Similar to the single H-bonded structure, the Al−O bond lengths of those waters involved in a hydrogen bond with O_W are significantly shorter than those in the bare $Al(H_2O)_6^{3+}$ cluster, 1.91 Å for $Al-O_x^+$ and $Al-O_y^+$, while the remaining Al−O distances are slightly longer, 1.94−1.95 Å. Because the asymmetric double H-bonded structure is the lowest in energy of the three $Al(H_2O)_6^{3+} + H_2O$ structures, it was used as the starting structure in each of the subsequent dissociations.

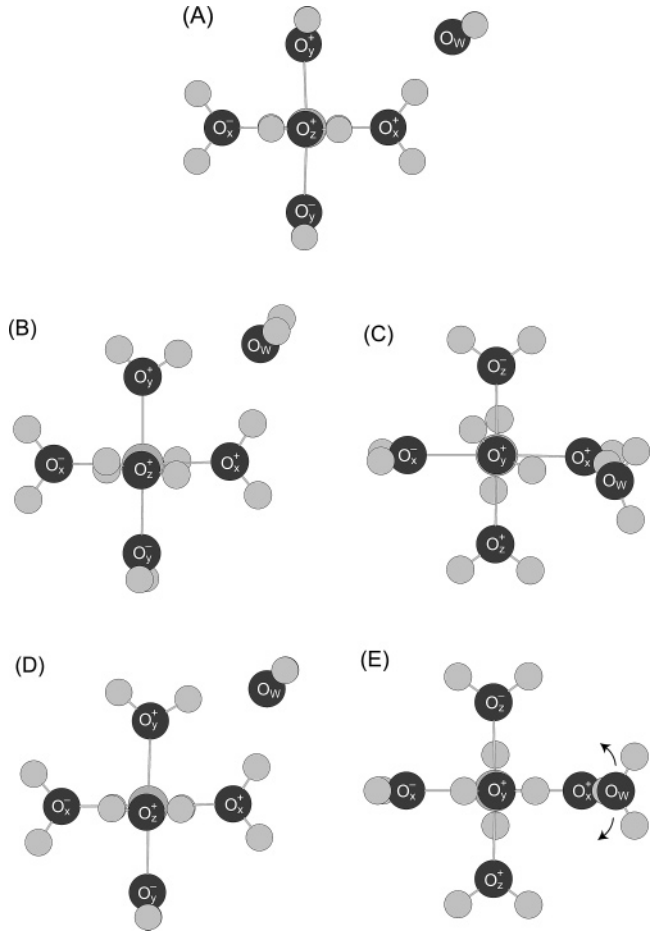

Figure 3. $Al(H_2O)_6^{3+} + H_2O$ clusters with (A) single H-bond; (B and C) double H-bond, without mirror plane symmetry (the minimum energy configuaration); (D and E) double H-bond, with mirror plane symmetry. Arrows in E show the imaginary mode.

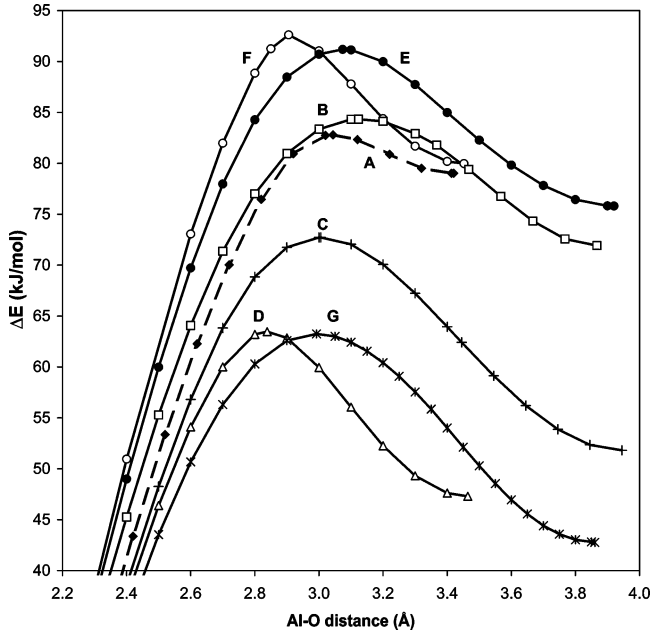

Figure 4. Comparing energy profiles for all symmetry-unique first-sphere water dissociations of $Al(H_2O)_6^{3+} + nH_2O$, $n = 0$ or 1. (A) bare $Al(H_2O)_6^{3+}$, (B) O_y^+, (C) O_y^-, (D) O_x^-, (E) O_x^+, C_1 symmetry, (F) O_x^+, C_s symmetry, (G) $O_z^{\pm}$.

Figure 3D and E shows a C_s-symmetric double H-bonded structure, which is the $Al(H_2O)_6^{3+} + H_2O$ structure used by Kowall et al.[18] It is 1.3 kJ/mol higher in energy than the

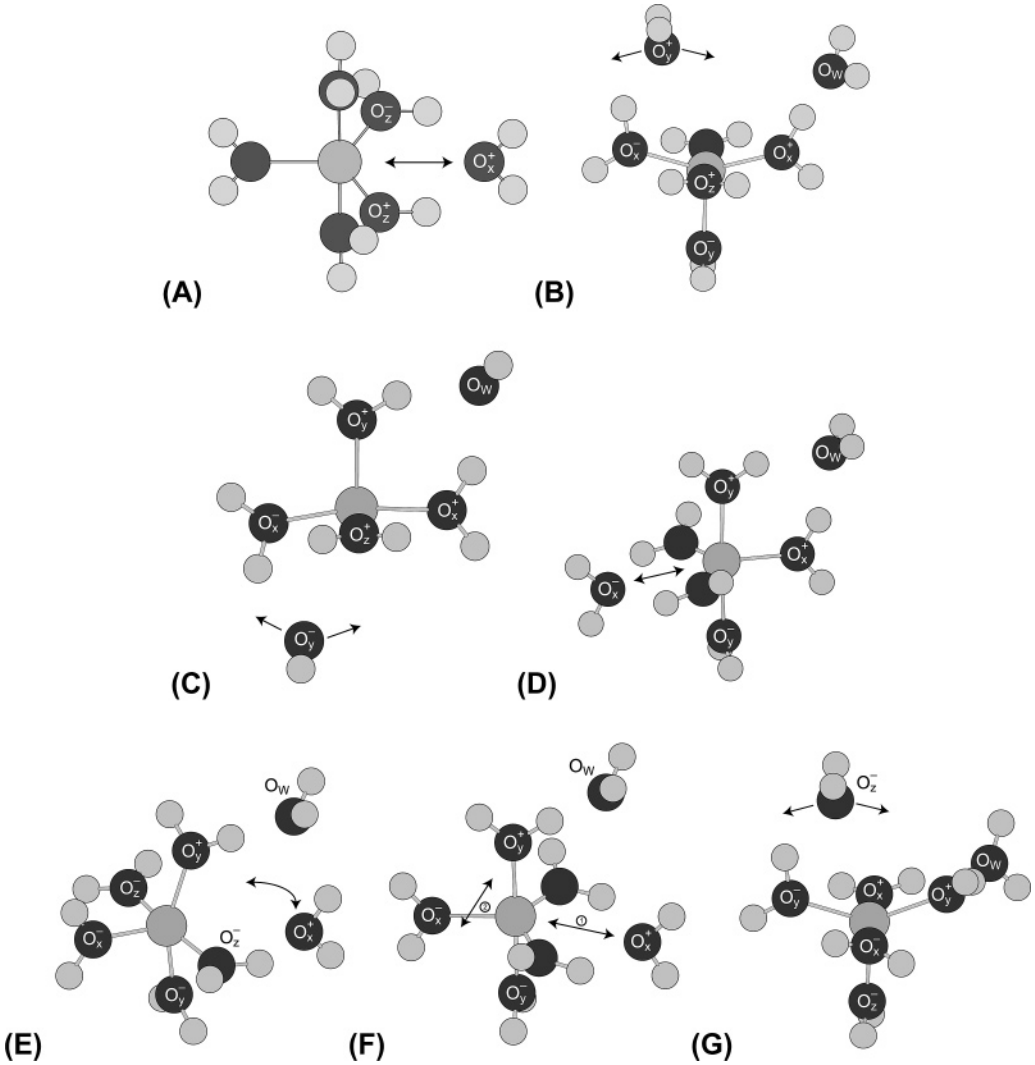

Figure 5. Transition-state/local maximum structures for first-sphere water dissociation from $Al(H_2O)_6^{3+} + nH_2O$, $n = 0$ or 1; letters correspond to the curves in Figure 4. (A) bare $Al(H_2O)_6^{3+}$ (from Figure 2), (B) O_y^+, (C) O_y^-, (D) O_x^-, (E) O_x^+, C_1 symmetry, (F) O_x^+, C_s symmetry, (G) $O_z^{\pm}$. Arrows show imaginary modes of vibration.

asymmetric structure. A vibrational frequency calculation shows that the symmetric double H-bonded structure has a single negative frequency (-100.9 cm^{-1}), corresponding to motion of O_W in and out of the *xy* plane (arrows in Figure 3E), while the asymmetric structure has none. This suggests that the symmetric double H-bonded structure is a transition state between the asymmetric structure and its *xy*-plane mirror image. The Al$-$O$_W$ distance in the symmetric structure is 3.75 Å, 0.023 Å longer than in the asymmetric structure. None of the other Al$-$O distances differ by more than 0.004 Å from those in the asymmetric structure. Although the O_y^+ and O_y^- waters are in plane with one another in bare $Al(H_2O)_6^{3+}$ and the single H-bonded structure, in the symmetric double H-bonded structure O_y^+ is rotated 90° with respect to O_y^- (Figure 3E), into the plane of the O_x^+ water, so that the second-sphere water sits in the *xy* plane. In the asymmetric structure, O_y^+ is only rotated about 30° with respect to O_y^-. This smaller twist of O_y^+ is likely the main reason for the difference in energy between the two double H-bonded structures: as O_W moves inward from the C_s-symmetric single H-bonded structure, the cost in energy for O_y^+ to twist by 30° while the unbound O_W molecule moves out of the *xy* plane in order to form an $O_W-O_y^+$ hydrogen bond is less than the cost to keep O_W in the *xy* plane and twist O_y^+ by 90°. Simply, O_W is easier to move because it is unbound.

3.2.2. Purely Dissociative Exchange for the $Al(H_2O)_6^{3+} + H_2O$ Structure. It has been shown both experimentally[22] and computationally[18,21] that water exchange in $Al(H_2O)_6^{3+}$ is I_d, more dissociative than associative. We simulate a purely dissociative (D) exchange by removing a first-sphere water (O_W') from $Al(H_2O)_6^{3+}$ by increasing the Al$-O_W'$ distance, forming a five-coordinated intermediate with two second-sphere waters (O_W and O_W'):

$$Al(H_2O)_6^{3+} + H_2O \rightarrow Al(H_2O)_5^{3+} + 2H_2O \qquad (2)$$

The principle of microscopic reversibility requires that the process of bringing the O_W water into the first coordination sphere should be a mirror image of the dissociation of O_W'; therefore, the intermediate $Al(H_2O)_5^{3+} + 2H_2O$ structure should be symmetric with respect to O_W and O_W'.

The addition of a second-sphere water to $Al(H_2O)_6^{3+}$ breaks the symmetry equivalence of the six first-sphere waters; thus, at least six distinct dissociations are possible. Which of these is the correct one leading to an exchange with O_W is not immediately obvious. Starting from the asymmetric double H-bonded structure, we seek which dissociation leads to a symmetric intermediate, and if more than one, which has the lowest energy transition state.

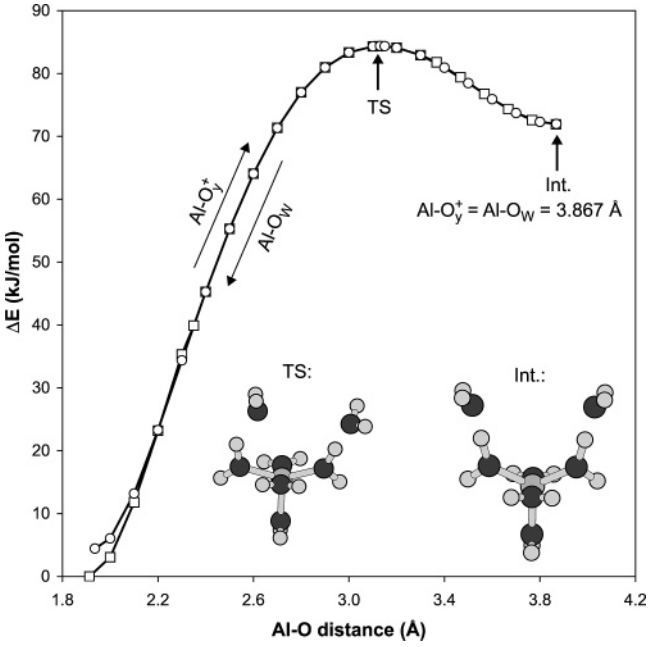

Figure 6. Exchange process on removing the O_y^+ first-sphere water from $Al(H_2O)_6^{3+} + H_2O$; squares are from asymmetric double H-bonded starting structure, and circles are from the single H-bonded starting structure. Forward movement on the curve corresponds to removing O_y^+ (ΔE vs $d(Al-O_y^+)$) while reverse movement corresponds to bringing in the second-sphere water O_W (ΔE vs $d(Al-O_W)$). The transition-state (TS) and intermediate (Int.) structures are labeled on the curve and shown in the inset.

Energy curves for each of the unique first-sphere dissociations are shown in Figure 4, along with the curve for bare $Al(H_2O)_6^{3+}$ for comparison. The corresponding local maximum energy structures are shown in Figure 5, with arrows indicating the normal modes of vibration corresponding to their negative frequencies. Not all of these local maxima are true transition states with a single negative frequency. Local maximum energies range from 64 to 93 kJ/mol, and intermediate (i.e., high d(AL−O) local minimum) energies from 43 to 80 kJ/mol. Only one of the six dissociations represented in Figure 4 fits the requirements for an exchange mechanism; however a second, not shown, was also found that does not use an Al−O distance as a reaction coordinate. Details of the individual dissociation pathways are discussed below.

A full list of first- and second-sphere Al−O distances and relative energies, for all $Al(H_2O)_6^{3+}$ and $Al(H_2O)_6^{3+} + H_2O$ starting structures, transition states, and intermediates is given in Table S1 in the Supporting Information.

3.2.3. Exchange through Dissociation of the O_y^+ Water. In Figure 4, the $Al(H_2O)_6^{3+} + H_2O$ dissociation curve whose local maximum is nearest to that of bare $Al(H_2O)_6^{3+}$ (curve A), at d(Al−O) = 3.04 Å and ΔE = 82.8 kJ/mol, is that which corresponds to removing water O_y^+ (curve B), which we shall refer to as the O_y^+ dissociation curve. The full curve is shown in Figure 6, with the transition-state (also shown in Figure 5B) and intermediate structures shown in the inset. The intermediate structure is symmetric with respect to the incoming and outgoing waters, and so O_y^+ dissociation is a potential exchange mechanism. In fact, this is the mechanism for Al^{3+} water exchange identified previously by Kowall et al.[18]

The second-sphere waters in the intermediate structure are single H-bonded to a square-pyramidal $Al(H_2O)_5^{3+}$ entity, with second-sphere Al−O distances of 3.87 Å. The transition-state energy is 84.3 kJ/mol (relative to the asymmetric double H-bonded starting structure) at $d(Al-O_y^+)$ = 3.12 Å, which compares well with the experimental exchange enthalpy of 84.7 kJ/mol measured by Hugi-Cleary et al.,[22] as well as the restricted Hartree−Fock result of Kowall et al.[18] of 85.4 kJ/mol, using a more specialized basis set. Hanauer et al.[21] report the same mechanism for Al^{3+} water exchange, derived from density functional calculations, albeit with a transition-state energy of only 48 kJ/mol. Analogous D mechanisms for water exchange are reported for Ni^{2+}[16], Mn^{2+} and Cu^{2+}[17], and Ga^{3+}[18].

During the dissociation, O_y^+ forms a single H-bond with water O_x^- while the O_x^-−H bond lengthens as $d(Al-O_y^+)$ increases. Above $d(Al-O_y^+) = 3.30$ Å, the O_x^- hydrogen shows a strong tendency to detach completely and bind with O_y^+, resulting in a $Al(H_2O)_4OH^{2+} + H_3O^+ + H_2O$ system. This was avoided by constraining the O_x^-−H bond length to its length in the $d(Al-O_y^+) = 3.30$ Å structure for the subsequent $d(Al-O_y^+) > 3.30$ Å optimizations. Others[26,32] have also reported that the $Al(H_2O)_5^{3+} + H_2O$ system tends toward deprotonation in its strong hydrogen bond between first- and second-sphere waters. This deprotonation is an artifact of having only one water in the second coordination sphere.

Figure 6 shows energy profiles for dissociation of O_y^+ from both the asymmetric double H-bonded (squares) and single H-bonded (circles) starting structures. For $Al-O_y^+$ distances greater than 2.1 Å, the energy difference between the two curves is less than 0.05 kJ/mol. The difference in structures is likewise small, and in both cases the final reaction intermediate is the same C_s-symmetric structure. However, there is a significant difference in the frequencies of the maximum energy structures: only the maximum on the asymmetric double H-bonded curve is a true transition state with a single negative frequency, corresponding to motion of O_y^+ toward and away from the cation. A normal mode corresponding to a twisting of the cluster in and out of the *xy* plane (similar to the vibration shown in Figure 3E), has a calculated frequency of +8.8 cm^{-1} in the asymmetric structure but −12.3 cm^{-1} in the C_s-symmetric structure, giving the latter two negative frequencies. The second negative frequency in this case is likely too small in magnitude to be significant. (By comparison, the smallest frequency is −107.7 cm^{-1} in the asymmetric versus −107.3 cm^{-1} in the symmetric structure.) The difference between a true transition state and a higher-order saddle point is sometimes very small, and the ability to distinguish one from the other may be sensitive to small differences in the starting structure.

As discussed above, the actual exchange mechanisms for octahedral ions in aqueous solution virtually always involve a concerted motion of both inner-sphere and outer-sphere waters, pathways that are neither purely A nor D[33]. As Rotzinger[26] notes, an I_d mechanism for exchange of water around a solvated ion like $Al(H_2O)_6^{3+}$ has never been seen in ab initio simulations, even in cases where experimental evidence for it is clear. He suggests that the cause of this might lie in the incomplete second coordination sphere, which we address below in larger ab initio and MD simulations.

3.2.4. Dissociation of the O_y^- Water. Aside from the O_y^+ dissociation, none of the $Al(H_2O)_6^{3+} + H_2O$ dissociations have an intermediate structure symmetric with respect to outgoing and incoming waters and thus do not lead directly to mechanisms for water exchange. However, study of the O_y^- dissociation leads to a closely related distortion pathway which is a possible exchange mechanism, with the reaction coordinate not an Al−O distance, but an O−Al−O bond angle.

The full O_y^- dissociation curve, curve C in Figure 4, is shown in Figure 7 (circles, labeled curve 7-1), with its intermediate structure (Int.) inset. In the intermediate, O_y^- is single H-bonded

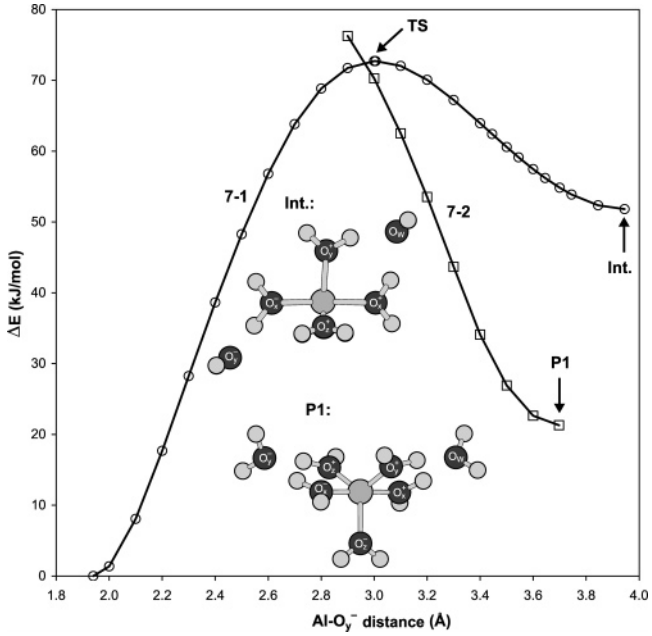

Figure 7. Energy profile for dissociation of water O_y^- from $Al(H_2O)_6^{3+} + H_2O$ (curve 7-1, circles), with the intermediate structure (Int.) shown in the inset. The $Al(H_2O)_5^{3+} + 2H_2O$ structure *P*1 is similar to the intermediate except that O_y^- is double H-bonded to the $Al(H_2O)_5^{3+}$ instead of single H-bonded. Curve 7-2 (square points) show the *P*1 cluster energy relative to undistorted $Al(H_2O)_6^{3+} + H_2O$ as $d(Al-O_y^-)$ is reduced.

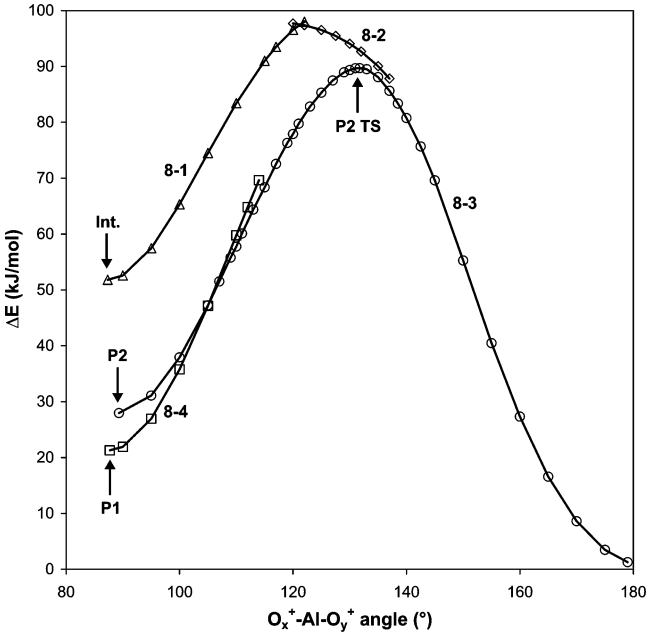

Figure 8. Energy profiles on opening the $O_x^+-Al-O_y^+$ angle in various $Al(H_2O)_5^{3+} + 2H_2O$ structures related to O_y^- dissociation. Curves 8-1 (triangles) and 8-2 (diamonds), from angular distortion of the O_y^- dissociation intermediate (Int.); curve 8-3, from angular distortion of structure *P*2 (shown in Figure 9); curve 8-4, from angular distortion of structure *P*1 (shown in the inset of Figure 7).

to O_x^-. The transition-state energy is 72.7 kJ/mol, and the intermediate energy is 51.8 kJ/mol, both values considerably smaller than those in the O_y^+ exchange process. Neither the intermediate nor the transition-state structures are symmetric with respect to the incoming and outgoing waters, so the unmodified O_y^- dissociation is unlikely to be a step in either an I_d or D exchange mechanism.

Those structures on the O_y^- dissociation curve to the right of the transition state, that is, with $d(Al-O_y^-) > 3.01$ Å, show a strong tendency to relax onto the second curve shown in Figure 7 (curve 7-2, squares) during optimization unless the starting structure is C_s symmetric with respect to the *xy* plane. In these relaxed structures, O_y^- is double H-bonded to O_x^- and either O_z^+ or O_z^-. The version of this structure with $d(Al-O_y^-)$ unconstrained is the left-hand endpoint of this curve, labeled *P*1, which has a much lower energy than the O_y^- intermediate (21.3 kJ/mol). In this respect, structures on the second half of the O_y^- dissociation curve, including the intermediate, are actually unstable.

A frequency calculation on the O_y^- intermediate shows that it actually has a single negative frequency (-99.6 cm^{-1}) corresponding to a twisting of O_y^- in and out of the *xy* plane, that is, toward the nearby O_z^+ or O_z^- waters, similar to that shown in Figure 3E. This is a normal mode distinct from that of the transition state's negative frequency, shown in Figure 5C. As in the case of the undistorted C_s-symmetric double H-bonded $Al(H_2O)_6^{3+} + H_2O$ structure, this result suggests that the O_y^- intermediate is actually the transition state between the two mirror image *P*1 structures, with O_y^- double H-bonded to O_x^- and O_z^+, or to O_x^- and O_z^-.

The *P*1 structure is symmetric with respect to the incoming and outgoing waters, with $d(Al-O_y^-) = d(Al-O_W) = 3.70$ Å, and so a continuous distortion pathway from $Al(H_2O)_6^{3+} + H_2O$ to *P*1 (or its reflection in the *xy* plane) would constitute a possible D exchange mechanism. We were unable to find such a pathway or its transition state because *P*1 structures with $d(Al-O_y^-) < 2.9$ Å relaxed back onto the original O_y^- dissociation curve during optimization. Any stable transition state for curve 7-2 lies higher in energy and lower in $d(Al-O_y^-)$ than the O_y^- transition state of curve 7-1.

3.2.5. Bond Angle Distortion in the O_y^- Intermediate and Related Structures. If the bond angle $\angle(O_y^+-Al-O_x^+)$ is increased in the square-pyramidal O_y^- intermediate, so that O_x^+ moves into the hole left by O_y^-, then the oxygen in O_W is gradually exposed to the high charge on the cation, and so O_W is drawn inward. Figure 8 shows the results of applying this distortion to the O_y^- intermediate and structure *P*1, through energy curves as a function of the bond angle. In each curve shown, the $Al-O_W$ distance decreases monotonically as $\angle(O_y^+-Al-O_x^+)$ increases.

In the case of *P*1 (curve 8-4, squares), beyond a bond angle of 114° the resulting structure is similar to those in the O_x^- dissociation (curve D in Figure 4), 15 kJ/mol lower in energy. For the O_y^- intermediate, however, the bond angle distortion could be continued all the way to 180°, resulting in the C_s-symmetric double H-bonded $Al(H_2O)_6^{3+} + H_2O$ structure with O_W in the O_x^- position and O_y^- in the second coordination sphere. However, the energy profile of the distortion is not continuous: as $\angle(O_y^+-Al-O_x^+)$ increases, the energy initially follows curve 8-1, jumps to curve 8-2 around 122°, and then to curve 8-3 above 137°. The discontinuities in both energy and structure are small, and at a sufficiently low angular resolution the path appears continuous; however, it has no transition state, or even a higher order saddle point, at its maximum energy. On curves 8-1 and 8-2, O_y^- is single H-bonded to O_x^-, whereas on curve 8-3, O_y^- is double H-bonded to O_x^- and O_x^+. The structural differences between curves 8-1 and 8-2 are even smaller, simply the orientation of the $O_z^{\pm}$ waters, as shown in Figure 9C and D.

If curve 8-3 is pushed backward, that is, to angles lower than 137°, then we find that it goes through a smooth maximum of 89.7 kJ/mol at 131.8°, labeled *P*2 TS in Figure 8 and shown in Figure 9B, to a local minimum at 90°, labeled structure *P*2, an

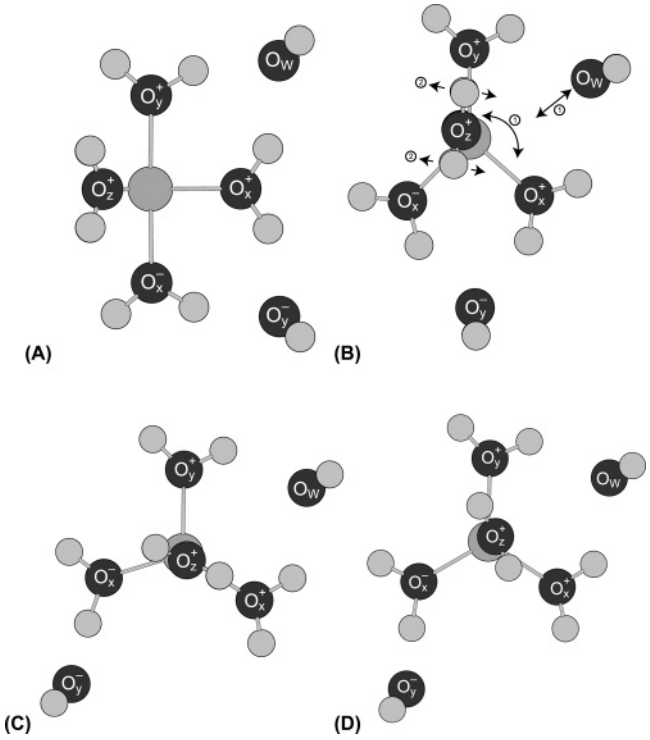

Figure 9. Structures from Figure 8. (A) Structure *P*2 − double H-bonded $Al(H_2O)_5^{3+} + 2H_2O$ structure, which is an intermediate in exchanging waters O_W and O_y^-. (B) *P*2 TS − "transition-state" structure for *P*2 path of water exchange (curve 8-3). Arrows show the two imaginary modes. (C and D) Structures with angle $O_x^+-Al-O_y^+$ equal to 122° from curves 8-1 and 8-2, respectively, in Figure 8.

$Al(H_2O)_5^{3+} + 2H_2O$ structure with C_{2v} symmetry (Figure 9A). The *P*2 structure is symmetric with respect to its outgoing and incoming waters; O_W is double H-bonded to O_x^+ and O_y^+, and O_y^- to O_x^+ and O_x^-. Its energy is 28.0 kJ/mol, considerably lower in energy than any stationary $Al(H_2O)_5^{3+} + 2H_2O$ structure we observed other than *P*1.

From the symmetry of *P*2, if the local maximum *P*2 TS has one negative frequency, then curve 8-3 would be a possible dissociative water exchange mechanism, following the curve from C_s-symmetric double H-bonded $Al(H_2O)_6^{3+} + H_2O$ at $\angle(O_y^+-Al-O_x^+) = 180°$ to *P*2, the intermediate, at $\angle(O_y^+-Al-O_x^+) = 90°$. The barrier height of 89.7 kJ/mol is relatively close (as compared with the other transition-state energies in Figure 4) to that of the O_y^+ mechanism discussed above, and considering the relatively simple level of theory, is also a good approximation to the experimental enthalpy. However, we find that the *P*2 TS structure has two negative frequencies, one (at $-138.4\ cm^{-1}$) corresponding to bending of $\angle(O_y^+-Al-O_x^+)$ and inward motion of O_W (motion 1 in Figure 9B), and a second (at $-48.7\ cm^{-1}$) corresponding to twisting of the mirror-symmetric $O_z^{\pm}$ waters and flexing in and out of the *xy* plane (motion 2 in Figure 9B). Nevertheless, it would be injudicious to dismiss it as a higher order saddle point irrelevant to water exchange. As discussed above, if the starting point of the O_y^+ exchange is the C_s-symmetric double H-bonded structure, which itself has a negative frequency corresponding to vibration about the plane of symmetry, then the negative frequency persists to the transition state, transforming it into a higher order saddle point with a structure nearly identical to the true transition state obtained from the asymmetric double H-bonded structure. Similarly, there may be a true *P*2 transition state nearby that we have been unable to find. Alternatively the second negative frequency may disappear with the inclusion of additional second-sphere waters. We show below that this *P*2/bond angle mechanism is also important in MD simulations of water exchange.

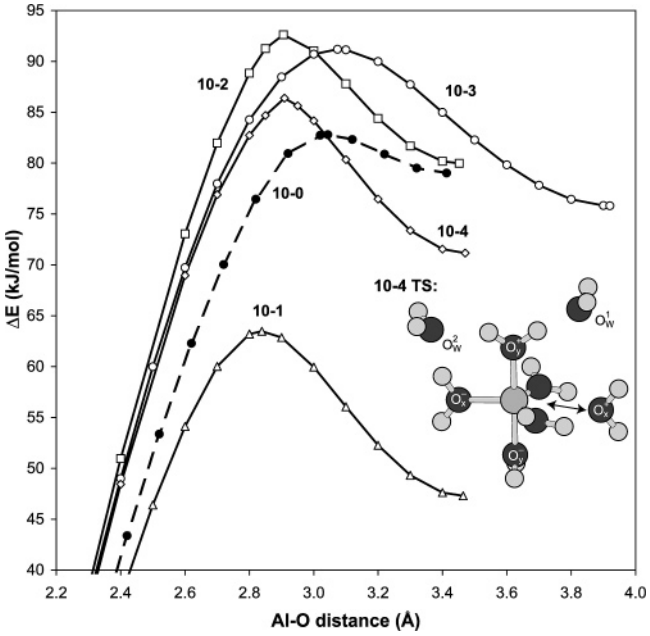

Figure 10. Energy profiles for the dissociation of first-sphere water O_x^+ and O_x^- from $Al(H_2O)_6^{3+} + nH_2O$, $n = 0$, 1, and 2. Curve 10-0 (dashed line), bare $Al(H_2O)_6^{3+}$; curve 10-1 (triangles), O_x^- from $Al(H_2O)_6^{3+} + H_2O$; curve 10-2 (squares), O_x^+ (C_s symmetric) from $Al(H_2O)_6^{3+} + H_2O$; curve 10-3 (circles), O_x^+ (asymmetric) from $Al(H_2O)_6^{3+} + H_2O$; curve 10-4 (diamonds), O_x^+ from $Al(H_2O)_6^{3+} + 2H_2O$ (energy relative to undistorted cluster). Its transition state is shown in the inset with arrows showing the imaginary mode.

3.2.6. Dissociation of the $O_x^{\pm}$ Waters. None of the remaining waters ($O_x^{\pm}$ and $O_z^{\pm}$), on dissociation, lead to transition states or intermediates that are symmetric with respect to incoming and outgoing waters; that is, their dissociations do not lead to an exchange mechanism. These dissociations are still interesting, however, in their relation to the other $Al(H_2O)_6^{3+}$ dissociation paths.

Figure 10 shows the energy dissociation profiles for waters O_x^+ and O_x^-. The O_x^- dissociation, curve D in Figure 4, is shown as curve 10-1 in Figure 10. The transition-state structure is shown in Figure 5D; the transition-state energy is 63.5 kJ/mol, and the intermediate energy 47.3 kJ/mol. It is a true transition state with a single negative frequency ($-129.0\ cm^{-1}$) corresponding to motion of the O_x^- toward and away from the cation (arrows in Figure 5D). The dissociation mechanism is identical to that in bare $Al(H_2O)_6^{3+}$, with the second-sphere water O_W relegated to the role of spectator (compare TS structures A and D in Figure 5).

Two mechanisms were found for dissociation of water O_x^+. Starting from the C_s-symmetric double H-bonded structure leads to a dissociation mechanism (curve F in Figure 4, curve 10-2 in Figure 10) analogous to that of the O_x^- water and of bare $Al(H_2O)_6^{3+}$. The maximum of the energy profile is 92.6 kJ/mol, and the intermediate energy is 80.0 kJ/mol. The structure at the maximum is shown in Figure 5F. It has two negative frequencies, one ($-122.8\ cm^{-1}$) corresponding to motion of O_x^+ toward and away from the cation (motion 1 in Figure 5E) and the other ($-124.7\ cm^{-1}$) to vibration in and out of the plane of symmetry (motion 2 in Figure 5E). This second "extra" negative frequency is analogous to that found in other dissociations starting from C_s-symmetric structures in the O_y^+ and O_y^- cases.

If we start from the asymmetric double-H-bonded structure, then we can find a suitable asymmetric O_x^+ dissociation (curve

10-3 in Figure 10) with only one negative frequency on its local maximum; however, the structure is not stable for $d(Al-O_x^+) > 2.5$ Å. Beyond this point, the $O_y^+-O_W$ hydrogen bond rotates during optimization so that O_W lies in the *yz* plane and is double H-bonded to O_y^+ and O_z^+, a structure that (with waters relabeled) occurs in the $O_z^\pm$ dissociation. To prevent this rotation, we restrict the dihedral angle $O_y^+-O_W-Al-O_x^+$ to its $d(Al-O_x^+) = 2.5$ Å value for subsequent points.

In the C_s-symmetric dissociation, the outgoing O_x^+ remains equidistant between the O_z^+ and O_z^- hydrogens, whereas in the asymmetric case, O_x^+ starts out slightly closer to the O_z^+ hydrogen, and is attracted in that direction as it moves farther away from the cation, forming a hydrogen bond. The curve reaches a maximum at $d(Al-O_x^+) = 3.08$ Å, 0.1 Å later than in the C_s-symmetric dissociation, with energy 91.2 kJ/mol, only 1.4 kJ/mol lower than that in the symmetric case. This structure (shown in Figure 5E) has only one negative frequency (-101.0 cm^{-1}) corresponding to motion of O_x^+ away from the cation, so the maximum is a true transition state.

Above $d(Al-O_x^+) = 3.2$ Å, a further dihedral angle must be frozen ($O_x^+-O_z^+-Al-O_y^-$ at its $d(Al-O_x^+) = 3.2$ Å value) to again prevent the structure from relaxing to a structure on the lower energy $O_z^\pm$ dissociation curve (in this case, by rotation of the $O_z^+-O_x^+$ hydrogen bond allowing O_x^+ to form a second hydrogen bond with O_y^-). The final highly constrained intermediate structure has $d(Al-O_x^+) = 3.92$ Å and $\Delta E = 75.8$ kJ/mol. The $Al-O_x^+$ distance is 0.5 Å longer than that in the symmetric intermediate, a result of O_x^+ being single H-bonded rather than double H-bonded.

3.2.7. Geometry of $O_x^\pm$ Dissociation Complexes and $Al(H_2O)_6^{3+} + 2H_2O$. We have seen that O_x^+ and O_x^- in the $Al(H_2O)_6^{3+} + H_2O$ cluster each have a dissociation mechanism similar to that seen for bare $Al(H_2O)_6^{3+}$ (momentarily ignoring the second negative frequency in the C_s-symmetric O_x^+ case), where the outgoing water remains equidistant between O_z^+ and O_z^- and the intermediate has a trigonal bipyramid structure. (All of the other $Al(H_2O)_5^{3+} + 2H_2O$ dissociation intermediates, including asymmetric O_x^+, are closer to square-pyramid structures.) The structures at the local maxima (Figure 5A for bare $Al(H_2O)_6^{3+}$, 6D for O_x^-, and 6D for C_s-symmetric O_x^+) differ primarily in the position or absence of the second-sphere water O_W.

If we include an additional second-sphere water double H-bonded to O_x^- and O_y^+, then the $O_x^\pm$ are once again symmetrically equivalent, and a dissociation of either will have structural features of both the O_x^- and O_x^+ dissociations with 1 second-sphere water. Curve 10-4 is the $Al(H_2O)_6^{3+} + 2H_2O$ dissociation, and the transition-state structure is shown in the inset. The local maximum has an energy of 86.4 kJ/mol and is a true transition state with one negative frequency at -120.9 cm^{-1}. (This latter point demonstrates that adding additional second-sphere waters can in some cases remove extra negative frequencies and turn higher order saddle points into transition states.) The intermediate structure occurs at has an energy of 71.2 kJ/mol.

The $Al(H_2O)_6^{3+} + 2H_2O$ dissociation has more in common with the O_x^- and C_s-symmetric O_x^+ dissociations in $Al(H_2O)_6^{3+} + H_2O$ than that of bare $Al(H_2O)_6^{3+}$. The outgoing water in the former three drops below the equatorial plane of the remaining first-sphere $Al(H_2O)_5^{3+}$, moving toward O_y^-, while in bare $Al(H_2O)_6^{3+}$, it remains in the plane. The O_y^+ is the *xz* plane mirror image of O_y^- in the bare $Al(H_2O)_6^{3+}$ dissociation, but rotated 90° to O_y^- in the other three. Finally, the $Al-O_x^\pm$ distances are all ~2.9 Å in the local maxima and 3.45−3.47 Å in the intermediate for the $O_x^\pm$ dissociations with second-sphere waters, but 3.044 Å and 3.413 Å, respectively, for the bare $Al(H_2O)_6^{3+}$ dissociation.

Despite similarities in structure, the dissociation energy curves in Figure 10 are widely separated in energy, with local maxima at 82.8 kJ/mol for bare $Al(H_2O)_6^{3+}$ (curve 10-0), 63.5 kJ/mol for O_x^- (curve 10-1), and 92.6 kJ/mol for O_x^+ (curve 10-2). The intermediate energies of bare $Al(H_2O)_6^{3+}$ and C_s-symmetric O_x^+, however, are very similar, 79.0 and 80.0 kJ/mol, respectively, while that of O_x^- is again much lower at 47.3 kJ/mol. The dissociation curve for $Al(H_2O)_6^{3+} + 2H_2O$ lies between the O_x^- and O_x^+ dissociations in energy, as one might expect.

The main contribution to the energy of the bare $Al(H_2O)_6^{3+}$ transition state is the breaking of the covalent $Al-O_x^+$ bond. In the C_s-symmetric O_x^+ dissociation of $Al(H_2O)_6^{3+} + H_2O$, the hydrogen bond between O_x^+ and O_W is also broken; it seems reasonable to assign the majority of the 8.4 kJ/mol difference between the C_s-symmetric O_x^+ local maximum and the bare $Al(H_2O)_6^{3+}$ transition state to the energy to break this hydrogen bond. After the maximum in each case, there is a formation of hydrogen bonds between O_x^+ and the $O_z^\pm$ waters, hence their similar intermediate energies.

If the formation and breaking of bonds were all there was to dissociation, then we would expect the O_x^- dissociation curve in Figure 10 to be very similar to that of bare $Al(H_2O)_6^{3+}$. Nevertheless, the O_x^- curve is anomalously low, 19 kJ/mol lower than bare $Al(H_2O)_6^{3+}$ at the transition state and 32 kJ/mol lower at the intermediate, even though O_W plays no apparent role in the dissociation.

3.2.8. Dissociation of the $O_z^\pm$ Waters. The O_z^+ and O_z^- waters are equivalent in C_s-symmetric $Al(H_2O)_6^{3+} + H_2O$ cluster but not in the lower energy asymmetric cluster. When starting from the asymmetric cluster, the O_z^+ and O_z^- dissociation curves remain separated by less than 2 kJ/mol up to $d(Al-O_z^\pm) = 2.7$ Å. Above this distance, the structures optimize to mirror images of one another with identical energies. Because the difference between dissociation of the ligands is negligible, we will consider only the O_z^- dissociation.

The O_z^- dissociation curve is labeled curve 11-1 (squares) in Figure 11. As the O_z^- water is removed, it moves toward and forms a hydrogen bond with the O_y^- water. The maximum at $d(Al-O_z^-) = 2.99$ Å and $\Delta E = 63.3$ kJ/mol is a true transition state with a single negative frequency (-123.8 cm^{-1}). Up to the transition state, the outgoing water remains in the *yz* plane, but at $d(Al-O_z^-) > 3.4$ Å the O_y^- -O_z^- hydrogen bond begins to rotate out of the plane toward O_x^+. At $d(Al-O_z^-) = 3.85$ Å, near the intermediate, O_z^- is close enough to the O_x^+ hydrogen that during optimization the structure relaxes to the lower energy curve 11-2 (circles), where O_z^- is double H-bonded to O_x^+ and O_y^-. To find the local minimum of curve 11-1, we restrict the $O_z^-O_y^-O_y^+O_W$ dihedral angle to its previous stable value. This intermediate structure is shown in Figure 12A.

The minimum on curve 11-2 is the structure labeled *P*3, an $Al(H_2O)_5^{3+} + 2H_2O$ structure with O_W double H-bonded to O_y^+ and O_x^+, and O_z^- double H-bonded to O_x^+ and O_y^- (Figure 12B). The intermediates in both O_z^- and asymmetric O_x^+ dissociation optimize to this structure when all bond distance and dihedral angle constraints are removed (albeit with a different labeling of oxygens in the O_x^+ case). Structure *P*3 is 8.2 kJ/mol lower in energy than the curve 11-1 intermediate, and it is symmetric with respect to the incoming and outgoing waters with $d(Al-O_z^-) = d(Al-O_W) = 3.66$ Å. Structure *P*3's lower energy is predominately due to both second-sphere waters

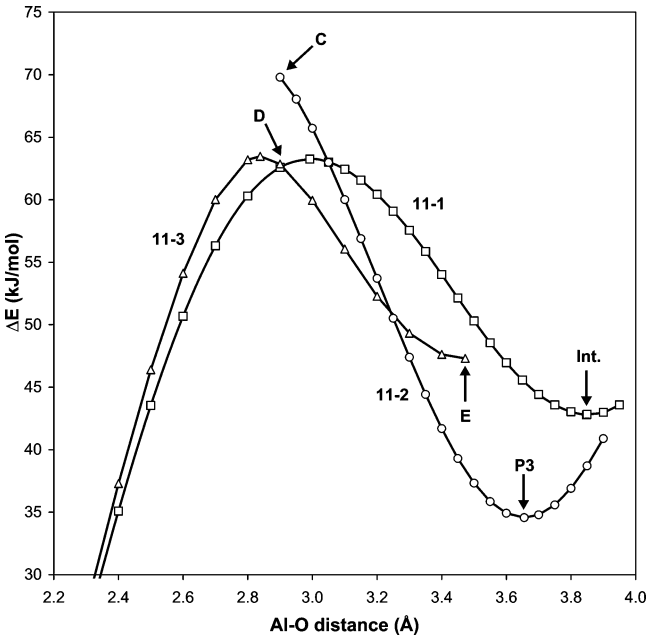

Figure 11. Energy profiles related to O_z^- dissociation. Curve 11-1 (squares), O_z^- dissociation; curve 11-2 (circles), alternate pathway from structure *P*3; curve 11-3 (triangles), O_x^- dissociation. Structures at labeled points are shown in Figure 12.

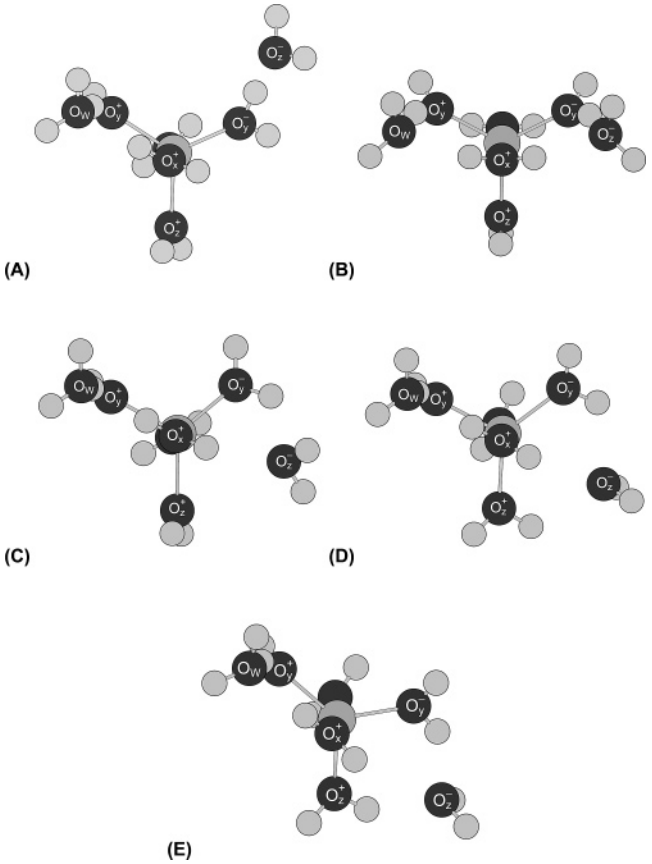

Figure 12. Structures from O_z^- dissociation corresponding to points labeled in Figure 11. (A) O_z^--dissociation intermediate; (B) *P*3 structure; (C) low $d(Al-O_z^-)$ endpoint of curve 12-2; (D and E) points on O_x^- dissociation curve (curve 11-3) with relabeled oxygens.

being double H-bonded, and it may be the preferred intermediate for O_z^- dissociation.

We were unable to find a continuous pathway from *P*3 to either the O_z^- transition state or undistorted $Al(H_2O)_6^{3+} + H_2O$ by varying the $Al-O_z^-$ distance or any bond angle involving O_z^- alone; such a pathway appears to require a more complex reaction coordinate. Varying the $Al-O_z^-$ distance from *P*3 produces curve 11-2. As O_z^- moves toward the cation in this configuration, the $Al-O_y^-$ bond tilts upward with respect to the plane defined by $O_W-O_y^+-Al-O_x^+$. The dissociated water stays mostly in this plane, and grows closer to O_z^+ as $d(Al-O_z^-)$ decreases (Figure 12C). Below $d(Al-O_z^-) = 2.90$ Å, the structure relaxes slightly during optimization and jumps from point C on curve 11-2 to point D on curve 11-3. Although there is a significant difference (~7 kJ/mol) in energy between these points, the two structures (Figure 12C and D) are very similar, differing primarily in the orientation of the protons on O_z^-, O_z^+, and O_x^-. Curve 11-3 is actually the O_x^- dissociation curve again, with the waters relabeled. Increasing the $Al-O_z^-$ distance leads to point E, which is the O_x^- intermediate (Figure 12E). The apparent close relation between the O_x^- and O_z^- dissociation paths may be the reason that their respective transition-state energies are nearly identical at 63.4 kJ/mol.

3.2.9. Summary: $Al(H_2O)_6^{3+} + H_2O$. Despite its simplicity, we have seen that the dissociation of a first-sphere water in the $Al(H_2O)_6^{3+} + H_2O$ system can follow at least five distinct paths with a wide range of transition-state energies. The link between energy and geometry for the transition states and intermediates is far from clear. The remaining five-coordinate structure may be either square-pyramidal, as in the O_y^+, O_y^-, $O_z^\pm$ or asymmetric O_x^+ dissociations, or trigonal-bipyramidal, as in the O_x^- dissociation. No energy preference is shown either structure because O_x^- and $O_z^\pm$ have almost identical transition-state energies although the two are of different five-coordinate geometries. Comparisons between like structures are not significantly more revealing; it is not apparent why the O_x^- transition state is so much lower than the bare $Al(H_2O)_6^{3+}$ or $Al(H_2O)_6^{3+} + 2H_2O$ transition states. It is not apparent why the $O_z^\pm$ transition state is lower than O_y^-, when in each case one hydrogen bond is formed and none are broken in a square-pyramidal structure.

A few specific conclusions are possible. The first is that a structure where a second-sphere water is hydrogen bonded to two adjacent first-sphere waters, that is, a double H-bond, is lower in energy than an equivalent structure where the second-sphere water hydrogen bonds to only one other water, that is, a single H-bond. The second-sphere Al−O distance is also significantly smaller in the double H-bond, around 3.6−3.7 Å compared to 3.9−4.0 Å in the single H-bond.

Second, the breaking of one hydrogen bond appears to contribute ~10 kJ/mol to the transition state (or local maximum) of a dissociation. This may account for the difference between the O_x^+ dissociation and bare $Al(H_2O)_6^{3+}$ (breaking the hydrogen bond between O_W and O_x^+ in the former), and the difference between the O_y^+ and O_y^- dissociations (where a bond between O_y^+ and O_W is broken in the former and none in the latter).

Most importantly for our original goal of studying water exchange, we have identified two possible mechanisms for exchange, the O_y^+ dissociation, with $d(Al-O_y^+)$ as reaction coordinate and the *P*2 dissociation (curve 8-3 in Figure 8) with the $\angle(O_y^+-Al-O_x^+)$ bond angle as reaction coordinate, both with similar transition states (ignoring again the second negative frequency for the latter process, which we believe would disappear with a full second coordination sphere). The fundamental difference between the two mechanisms is that in the O_y^+ dissociation incoming and outgoing waters are cis to one another, while in the other, incoming and outgoing waters are trans to one another. We shall use the cis and trans labels to refer to the two mechanisms in subsequent discussions.

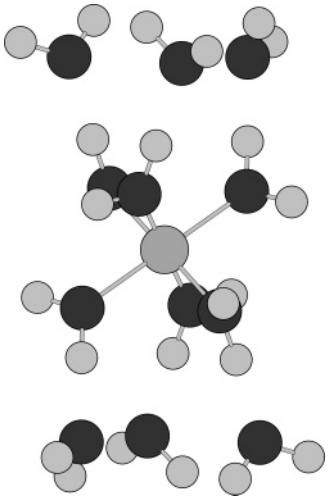

Figure 13. $Al(H_2O)_6^{3+} + 6H_2O$ with S_6 symmetry (6W structure). Each first-sphere water is equivalent and single H-bonded to one second-sphere water.

3.3. Clusters with Larger Second-Hydration Spheres. The small size of the $Al(H_2O)_6^{3+} + H_2O$ model introduces an artificial distinction to the simulation. Some first-sphere waters are hydrogen bonded to O_W and others are not, and those others differ from one another in their spatial relationships with O_W, and as has been demonstrated, this creates significant differences in the processes of dissociation and exchange. Yet, in an ideal static model of a solution, each first-sphere water in the equilibrium structure of $Al(H_2O)_6^{3+}$ should be equivalent; each should be hydrogen-bound to the same number of second-sphere waters in the same configuration. The simplest way to model this, given two sites for H-bonding on each water, is with each first-sphere water H-bonded to either one or two second-sphere waters, that is, with $Al(H_2O)_6^{3+} + nH_2O$ for $n = 6$ or 12.

A full list of first- and second-sphere Al−O distances and relative energies, for all $Al(H_2O)_6^{3+} + nH_2O$ starting structures, transition, states and intermediates where $n > 1$, is given in Table S2 of the Supporting Information.

3.3.1. Exchange through Dissociation in $Al(H_2O)_6^{3+} + 6H_2O$. Figure 13 shows the optimized structure, which we will refer to as 6W, for $Al(H_2O)_6^{3+} + 6H_2O$, where each first-sphere water is single H-bonded to exactly one second-sphere water. There are no secondary H-bonds between the second-sphere waters. The undistorted structure has point group symmetry S_6, with the second-sphere waters arranged in layers above and below the first coordination sphere. The first-sphere Al−O bond length is 1.91 Å, shorter than that in bare $Al(H_2O)_6^{3+}$, while the second-sphere Al−O distance is 4.08 Å, slightly longer than $d(Al-O_W)$ in the single H-bonded $Al(H_2O)_6^{3+} + H_2O$ cluster (3.95 Å). The central AlO_6 octahedron is flattened slightly normal to the cluster's threefold axis of symmetry, with a flattening angle of 55.0° (as compared with 54.74° in an ideal octahedron). The equilateral triangles formed by the second-sphere waters are rotated 22.6° with respect to the adjacent triangle of first-sphere waters. When dissociating a first-sphere water, we designate the removed water as O_x^+ and label the other first-sphere waters accordingly.

Figure 14 compares dissociation profiles for the 6W structure (curve 14-1, squares) with bare $Al(H_2O)_6^{3+}$ (curve 14-2, triangles) and O_y^+ in $Al(H_2O)_6^{3+} + H_2O$ (curve 14-3, circles). The 6W dissociation is essentially the same as the O_y^+ dissociation in $Al(H_2O)_6^{3+} + H_2O$, with the outgoing water single H-bonded to the central $Al(H_2O)_5^{3+}$, cis to the incoming water. The transition-state and intermediate structures are shown in Figure 15, with the incoming water, H-bonded to O_z^+, labeled O_W. For $d(Al-O_x^+) > 2.9$ Å, the dihedral angle $O_x^+-O_z^--O_z^+-O_W$ is constrained to zero to prevent a rearrangement of the second-sphere waters during optimization involving the

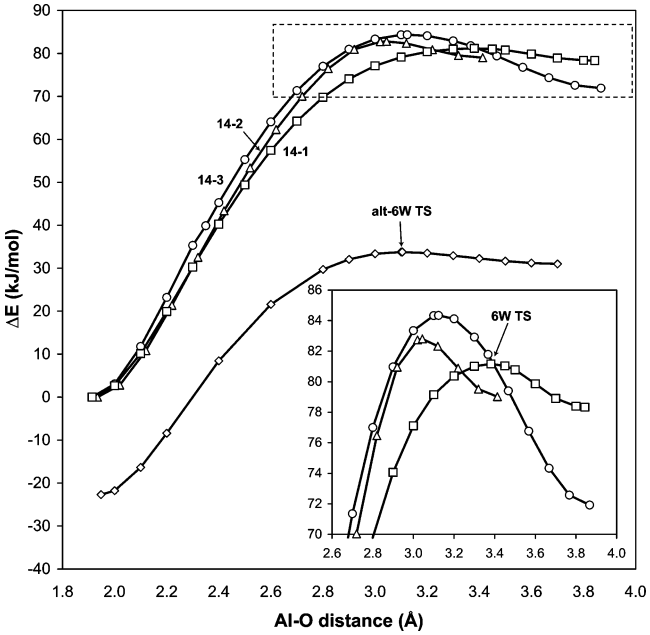

Figure 14. First-sphere water dissociation from $Al(H_2O)_6^{3+} + nH_2O$ clusters, $n = 0$, 1 or 6. Curve 14-1 (squares), $Al(H_2O)_6^{3+} + 6H_2O$ (6W structure); curve 14-2 (triangles), bare $Al(H_2O)_6^{3+}$; curve 14-3 (circles), O_y^+ dissociation from $Al(H_2O)_6^{3+} + H_2O$; curve 14-4 (diamonds), $Al(H_2O)_6^{3+} + 6H_2O$, alt-6W structure, relative to undistorted 6W. An expansion of the region shown in the dotted box is shown in the inset.

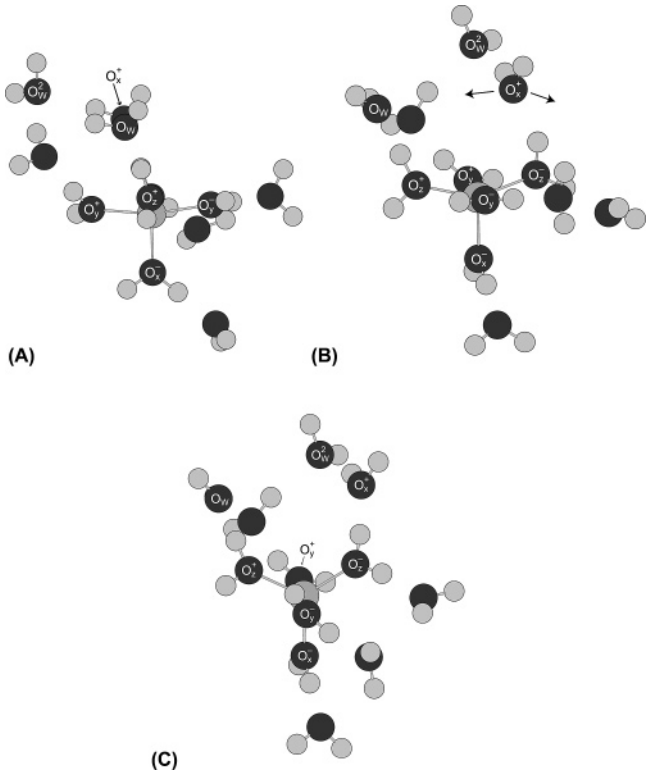

Figure 15. Transition-state (A and B) and intermediate structure (C) for dissociation of a first-sphere water (O_x^+) from $Al(H_2O)_6^{3+} + 6H_2O$, 6W structure. The second-sphere water that exchanges with O_x^+ is labeled O_W; the water labeled O_W^2 is H-bonded to O_x^+ and is pushed out of the second sphere. Arrows in B show the imaginary mode of vibration.

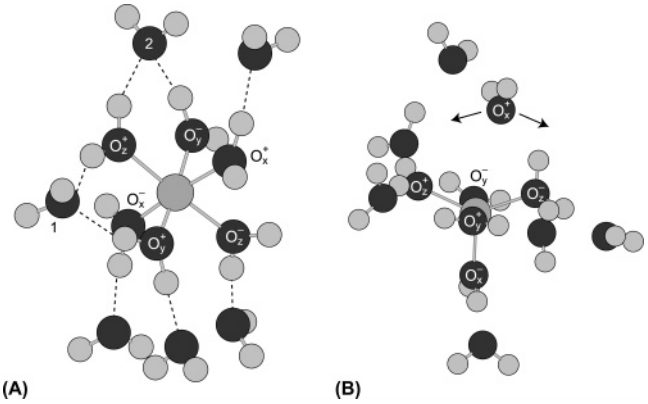

Figure 16. Alternate configuration for $Al(H_2O)_6^{3+} + 6H_2O$, structure alt-6W. (A) Undistorted; hydrogen bonds are shown as dotted lines, and second-sphere waters rearranged from structure 6W are labeled 1 and 2. (B) Transition state for dissociation of O_x^+. Arrows in B show the imaginary mode of vibration.

formation of double H-bonds, which drops the structure onto the lower energy curve 15-4. The unrestricted dihedral angle decreases from 20.7° in the undistorted 6W structure to −0.05° at $d(Al-O_x^+) = 2.9$ Å.

The transition-state energy of the 6W dissociation is 81.2 kJ/mol at $d(Al-O_x^+) = 3.381$ Å (negative frequency -37.7 cm^{-1}), a much higher distance than any of the transition states for $Al(H_2O)_6^{3+} + H_2O$, which tend to cluster around 3.0 Å (see Table S1 in the Supporting Information), the highest being O_y^+ at 3.12 Å and the lowest O_x^- at 2.84 Å. The intermediate energy is 78.3 kJ/mol, at $d(Al-O_x^+) = 3.84$ Å. Unlike the O_y^+ intermediate, the 6W intermediate is not exactly symmetric with respect to the outgoing and incoming waters because of the arrangement of the five spectator waters in the second sphere. For example, $d(Al-O_W)$ in the intermediate is 3.89 Å, slightly longer than $d(Al-O_x^+)$.

As O_x^+ moves farther from the cation, the second-sphere water to which it is H-bonded (labeled O_W^2 in Figure 15) is carried with it and is pushed out of the second sphere, to 5.51 Å from the aluminum in the intermediate. It forms a second H-bond with another spectator water but remains linked to O_x^+ because of the stiffness of the hydrogen bond. The dissociation of a water from the first sphere requires a reorganization of the second and higher coordination spheres.

Although the dissociation mechanism resembles the cis O_y^+ dissociation, from the inset of Figure 14 we can see that the energy scale for 6W more closely resembles the dissociation of bare $Al(H_2O)_6^{3+}$. The small difference between the 6W transition state and intermediate state, 2.9 kJ/mol, makes this portion of the energy curve particularly flat. This flatness may in part be due to the dihedral constraint. In most of the $Al(H_2O)_6^{3+} + H_2O$ dissociations, this difference is 10−20 kJ/mol.

If the $O_x^+-O_z^--O_z^+-O_W$ dihedral is unconstrained above $d(Al-O_x^+) = 2.9$ Å, then the formation of double H-bonds during optimization drops the structure onto curve 15-4, over 30 kJ/mol lower in energy. The minimum of curve 15-4 is the structure shown in Figure 16A, which we label the alt-6W structure. The first-sphere water being dissociated, O_x^+, is clearly no longer equivalent to the other first-sphere waters. Two of the second-sphere waters, labeled 1 and 2 in Figure 16A, have formed additional hydrogen bonds in a rearrangement of the top layer of waters in the 6W structure (compare Figure 13). Water 1, formerly single H-bonded to O_z^+, drops below the upper plane of second-sphere waters and is now double H-bonded to O_z^+ and O_y^+, while

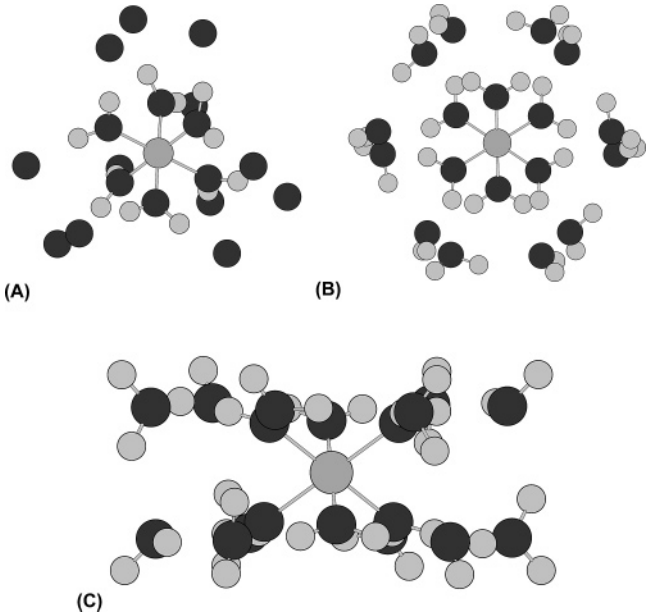

Figure 17. $Al(H_2O)_6^{3+} + 12H_2O$ structures. (A) 12W-T, with protons on the second sphere waters hidden for clarity; (B) structure 12W-S6, top view; (C) structure 12W-S6, side view.

water 2, formerly single H-bonded to O_y^-, is now double-H bonded to O_y^- and O_z^+. The undistorted alt-6W cluster is 22.7 kJ/mol lower in energy than undistorted 6W.

Curve 15-4 has a transition state of 56.5 kJ/mol (relative to undistorted alt-6W) at an $Al-O_x^+$ distance of 3.11 Å (negative frequency -58.9 cm^{-1}); the structure is shown in Figure 16B. The intermediate occurs at 53.7 kJ/mol at $d(Al-O_x^+) = 3.721$ Å. As in the 6W dissociation, the energy difference between the transition state and the intermediate state is small, only 2.8 kJ/mol. The intermediate and transition-state structures, as well as the transition-state energy, are very similar to those of the $O_z^{\pm}$ dissociation for $Al(H_2O)_6^{3+} + H_2O$, with O_x^+ acting as $O_z^{\pm}$ and water 1 (Figure 16A) as O_W. Near the alt-6W intermediate, there is a strong tendency for the outgoing water to tilt downward and form a double H-bond (in this case with O_z^- and O_y^-) in an analogue of the *P*1 structure (inset of Figure 7), not the *P*3 structure (Figure 12B) as in the $O_z^{\pm}$ dissociation. The 6W *P*1 analogue has an energy of 6.0 kJ/mol relative to 6W, 28.7 kJ/mol relative to alt-6W. Despite the initial symmetry of the first-sphere waters in the 6W structure, there is as much potential for alternative dissociation pathways here as with $Al(H_2O)_6^{3+} + H_2O$, due to the many different ways of reconfiguring the hydrogen-bonding network of the six second-sphere waters.

3.3.2. Dissociation in $Al(H_2O)_6^{3+} + 12H_2O$. In the $Al(H_2O)_6^{3+} + 6H_2O$ clusters, each of the six first-sphere waters had one "open" hydrogen not involved in a hydrogen bond. In $Al(H_2O)_6^{3+} + 12H_2O$, all first-sphere waters are fully hydrogen bonded.

Two different structures were found for undistorted $Al(H_2O)_6^{3+} + 12H_2O$. The first is shown in Figure 17A, with the second-sphere hydrogens hidden for clarity. This structure, 12W-T, has tetrahedral (*T*) point group symmetry, with the 12 second-sphere waters arranged into four truncated-tetrahedral "faces". Each face resembles one of the second-sphere water layers in the 6W structure (compare Figure 13). All second-sphere waters are single-H bonded to one first-sphere water, with Al−O distances of 4.14 Å. The first-sphere Al−O bond length is 1.91 Å.

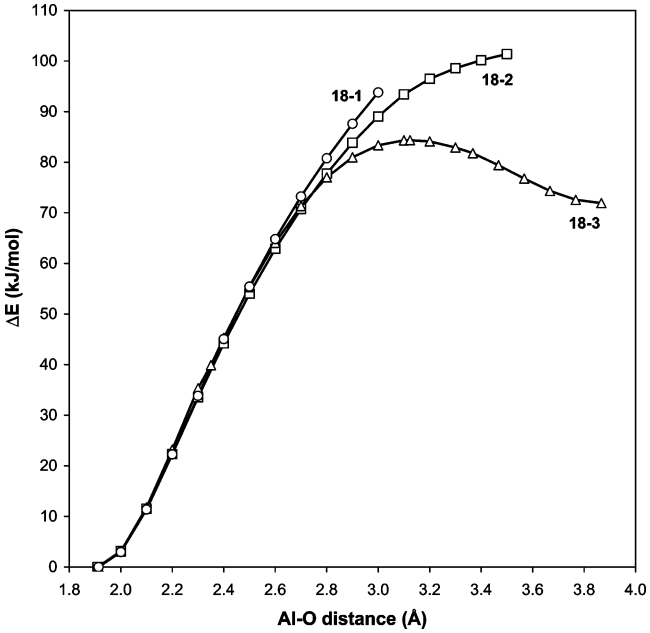

Figure 18. First-sphere water dissociation from $Al(H_2O)_6^{3+} + 12H_2O$ clusters. Curve 18-1 (circles), the 12W-S6 structure; curve 18-2 (squares), the 12W-T structure; curve 18-3 (triangles), O_y^+ dissociation from $Al(H_2O)_6^{3+} + H_2O$.

The second undistorted $Al(H_2O)_6^{3+} + 12H_2O$ structure, 12W-S6, has point group symmetry S_6, and is lower in energy than the 12W-T structure by 12.6 kJ/mol. The structure is shown in Figure 17B and C. All 12 second-sphere waters are arranged in a narrow layer (Figure 17C), with the central AlO_6 polyhedron slightly flattened compared to a true octahedron ($\psi = 55.9°$). Each second-sphere water is double H-bonded to one first-sphere water and one other second-sphere water. There are two inequivalent groups of second-sphere waters, with Al−O distances of 4.042 and 4.067 Å, which alternate along the perimeter of the structure. Each first-sphere water is hydrogen bonded to one of each group. The first-sphere Al−O bond length is 1.91 Å, similar to the 12W-T and 6W structures. All six first-sphere waters are equivalent in both 12W structures.

These two structures for a 12-water second coordination sphere have been found previously[32,34,35] for both Al^{3+} and Mg^{2+}. In each case, the 12W-S6 structure is the lowest in energy. The lower energy and second-sphere Al−O distances in 12W-S6 are consistent with our previous observations about double H-bonded versus single H-bonded second-sphere waters.

Although the 12W-S6 structure is lower in energy, the distinct flatness of the structure introduces a special direction, the axis of threefold symmetry normal to the plane. (12W-S6 has this in common with the 6W structure.) For Al^{3+}(aq) in the bulk liquid, we expect that with thermal motion the second and higher coordination spheres will be isotropic on average, suggesting that the undistorted 12W-S6 structure may be more appropriate as a section of a solid rather than a solution.

Figure 18 shows energy profiles for dissociation of a first-sphere water from each 12W cluster, along with the O_y^+ dissociation in $Al(H_2O)_6^{3+} + H_2O$ for comparison. We were unable to find a transition state or intermediate for either starting structure. At Al−O distances above 3.0 Å for 12W-S6 and 3.5 Å for 12W-T, a water is ejected from the second sphere for a discontinuous drop in energy. At the curves end points the energies are already larger, 93 kJ/mol for 12W-S6 and 101 kJ/mol for 12W-T, than previous exchange or dissociation barrier energies.

The existence of a transition state and intermediate depends on the outgoing first-sphere water finding a position in the second coordination sphere and forming one or more hydrogen bonds with other waters; the outgoing water is attracted by a hydrogen not involved in a hydrogen bond, as seen in the various $Al(H_2O)_6^{3+} + H_2O$ dissociations. In both the 12W-S6 and 12W-T structures, there is no available space in the second coordination sphere because all available hydrogen-bonding sites are occupied. The problem is that the existing network of static hydrogen bonds in these structures is too rigid to allow a dissociating water to enter the second coordination sphere. This problem can be alleviated by allowing thermal motion of the second sphere to break up the rigidity of the hydrogen bond network, that is, by switching to molecular dynamics simulations.

3.4. Molecular Dynamics. Ab initio structure optimizations are essentially static and can only give limited amounts of information about dynamic processes like dissociation or water exchange. A prerequisite for dissociating a water ligand from the aluminum cation's first coordination sphere is the existence of a hole in the second coordination sphere into which the dissociating ligand can move. In the static ab initio simulations, the network of intra-second-sphere and first sphere−second sphere hydrogen bonds is too rigid to accommodate the dissociating water ligand without an energetically discontinuous rearrangement of the second coordination sphere.

In a molecular dynamics (MD) simulation, however, the molecules in the second and outer coordination spheres are in constant thermal motion and can more readily reorganize to accommodate the outgoing water. Another advantage is the ability to have many more molecules in the system (a full outer coordination sphere transitioning into bulk water, given a small enough core system and a large enough box for the simulation) than in an ab initio simulation. However, structures obtained from MD (e.g., intermediate or transition-state structures, the structure of the second coordination sphere) are in one sense more approximate than those from ab initio calculations, being either averages over many time steps or snapshots from a single time step deemed representative, rather than energy-minimized structures.

More extensive MD simulations on water exchange in Al^{3+} with CLAYFF, using sampling and weighted histogram analysis, have been performed previously,[36] yielding a calculated exchange enthalpy for $Al(H_2O)_6^{3+}$ of 101.5 kJ/mol.

The aluminum cation was fixed in the center of a box, ~18.5 Å per side, with periodic boundary conditions, and filled with 215 water molecules. Each simulation was run for 1000 time steps over 1 ps. Dissociation of a first-sphere water was simulated in a way similar to that of the ab initio simulations, by gradually increasing the fixed Al−O distance for a chosen first-sphere water. For each Al−O distance, the simulation was repeated 2000 times.

In the unconstrained simulation (i.e., with no fixed Al−O distance) the average geometry of the $Al(H_2O)_6^{3+}$ cluster is octahedral, with no significant difference between the six ligands. Figure 19A shows the partial radial distribution function (RDF) for oxygen atoms with the origin at the aluminum cation, derived from a single 1 ps simulation. The sharp, high peak corresponds to the Al−O bond length in $Al(H_2O)_6^{3+}$, with peak value 1.85 Å, mean 1.87 Å, and standard deviation 0.03 Å. This bond length is considerably shorter than that in any of the ab initio clusters (1.93 Å in bare $Al(H_2O)_6^{3+}$, 1.91 Å in 6W and the two 12W structures), which is an artifact of CLAYFF.[36] The octahedron is not flattened as in the 6W or 12W-S6

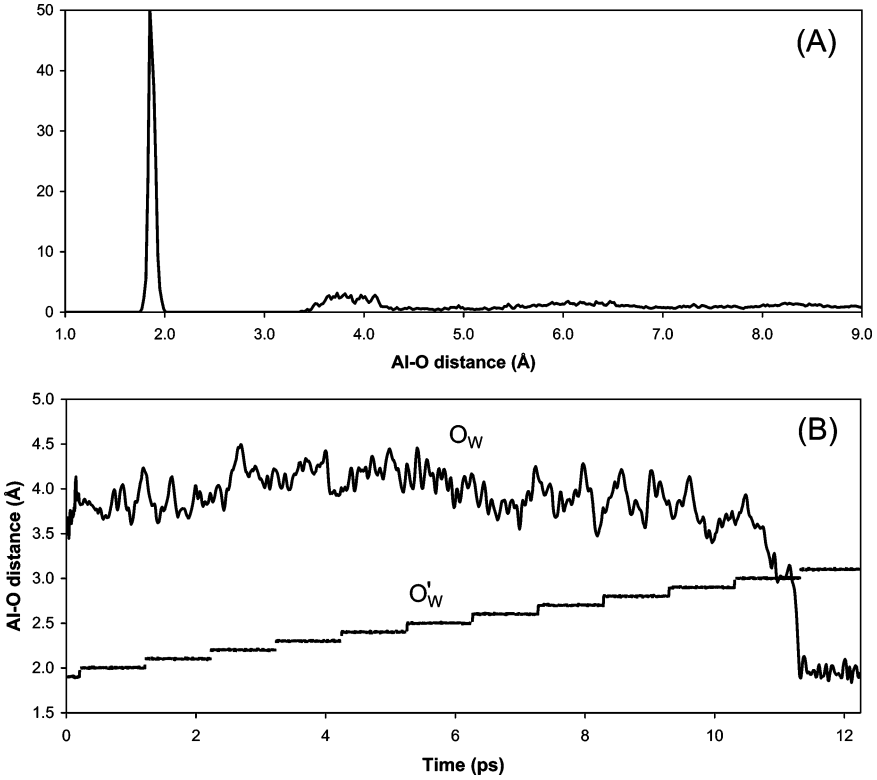

Figure 19. (A) Radial density function (RDF) of Al−O distances in GROMACS MD simulation, undistorted $Al(H_2O)_6^{3+}$. (B) Forced dissociation of a first-sphere water (O_W') and its subsequent replacement by a second-sphere water (O_W).

structures. The first coordination sphere is stable over the length of the simulation, and no spontaneous exchange between the first and second coordination spheres was observed.

The second coordination sphere, however, was relatively fluid, both in structure and membership. The second sphere can be seen in Figure 19A as the small broad peak between roughly 3.5 and 4.5 Å. (The second coordination sphere peak is noisy because of the short simulation time.) Unlike between the first and second coordination spheres, there is no sharp edge between the second and higher coordination spheres.

In general, however, there are 12 waters hydrogen bonded to the first sphere and few waters closer to the cation that are not, in agreement with previous simulations[37] that show 12 waters in the second coordination sphere. The second sphere has neither a 12W-T or 12W-S6 structure but is much more disordered, although most waters are single rather than H-bonded, like the 12W-T structure. Although double H-bonding is energetically preferred in ab initio simulations, it is not often seen in MD simulations because the energy difference between single and double H-bonded configurations is of similar magnitude to the thermal energy, $kT = 2.4$ kJ/mol at 300 K, while ab initio ΔE between single and double H-bonded $Al(H_2O)_6^{3+} + H_2O$ is 3.1 or 4.4 kJ/mol, depending on double H-bonded symmetry.

Figure 19B shows the result of a sequence of consecutive simulations where the fixed Al−O distance for a water originally in the first sphere (O_W') is increased gradually. Here the final state of each 1 ps simulation is used as the initial state of the next simulation with increased $d(Al-O_W')$, while in subsequent simulations, each simulation was started from the same initial state. The curve labeled O_W' is the $Al-O_W'$ distance over time. Eventually, the hole left in the first sphere by the O_W' is large enough that one of the second-sphere waters, O_W, which has been keeping between 3.5 and 4.5 Å from the aluminum, takes its place.

Figure 20A shows the fraction of simulations in which an exchange occurred sometime during the simulation's 1 ps duration, as a function of the constrained $Al-O_W'$ distance. Each data point represents 2000 simulations. The number of exchanges increases the farther O_W' is held from the cation; the larger the hole in the first sphere, the greater the chance that a second-sphere water will be able to fill it. The dependence is well fit by a sigmoidal function

$$N_{\text{exchanges}}/N_{\text{total}} = 1/\{1 + \exp[-(x - x_0)/\Delta x]\} \qquad (3)$$

where $N_{\text{exchanges}}$ is the number of simulations where a water exchange occurred out of a total N_{total} simulations, x is the constrained $Al-O_W'$ distance, and x_0 and Δx are parameters. The fitted values of the parameters in Figure 20A are $x_0 = 2.946(6)$ Å, $\Delta x = 0.074(5)$ Å, with $\chi^2 = 0.0008$. Both x_0 and Δx are expected to have some dependence on the length of the simulation.

The parameter x_0 is the $Al-O_W'$ distance where an exchange will occur in exactly half of the simulations and is quite close to 3.0 Å. Many of the dissociation and exchange mechanisms observed in the ab initio simulations had their transition states or local maxima near 3.0 Å. It is thus tempting to identify x_0 as the $d(Al-O_W')$ of a D or I_d exchange transition state. However, this supposes that this hypothetical transition-state structure has a 50% probability of proceeding forward to a completed exchange (O_W moving in to replace O_W'), or slipping back to its starting configuration (O_W' moving back into the first sphere), that is, that the transmission coefficient is 0.5. Although this is an attractive picture, it is known that the transmission coefficients for exchange processes, as calculated by the reactive flux method, are generally much smaller than 0.5.[36,38,39] In addition, although x_0 appears to match $d(Al-O_W')$ of the ab initio transition states, the fact that the equilibrium Al−O bond lengths in $Al(H_2O)_6^{3+}$ are about 0.1 Å smaller in the MD

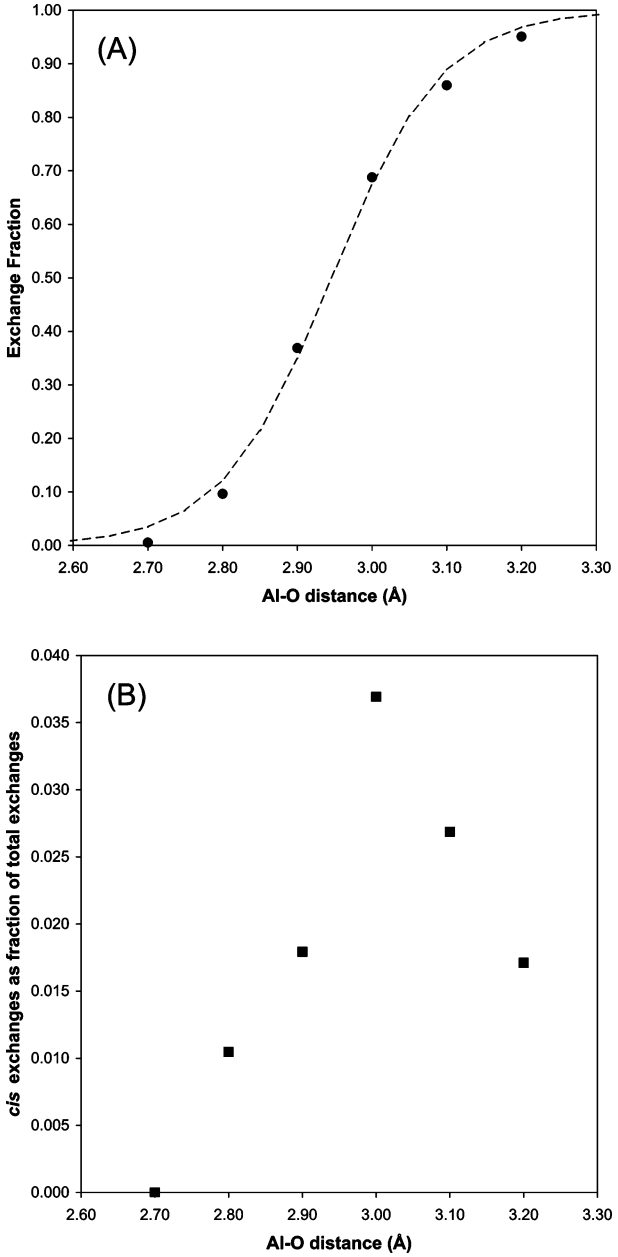

Figure 20. Dependency of water exchange characteristics as a function of the constrained Al−O_W' distance. (A) Total fraction of simulations where water exchange ocurrs, with fitted sigmoidal curve (dashed line); (B) cis exchanges as a fraction of the total exchanges.

simulations suggests that a similar difference might be expected in the Al−O distances of a transition state or intermediate.

Examining the actual individual water exchanges, we find two different mechanisms, one trans, like the *P*2 O_y^- exchange in $Al(H_2O)_6^{3+} + H_2O$ (Figure 8, curve 8-3, and Figure 9), and one cis, that looks the O_y^+ exchange (Figure 6). Representative examples of the two mechanisms as seen in MD are shown in Figure 21, each for a simulation with fixed $d(Al-O_W') = 3.0$ Å; the waters are labeled O_W, O_x^+, O_x^-, and so forth to correspond with the equivalent mechanism in the $Al(H_2O)_6^{3+} + H_2O$ ab initio simulations. Figure 21A−C shows the first sphere immediately before, during (when both $d(Al-O_y^-)$ and $d(Al-O_W)$ are 3.0 Å), and after the trans exchange, while Figure 21D shows the first sphere during the cis exchange (again, when both $d(Al-O_y^+)$ and $d(Al-O_W)$ are 3.0 Å). Both these mechanisms are of the intermediate I_d type rather than the purely dissociative D type, seen in the ab initio simulations. The cis

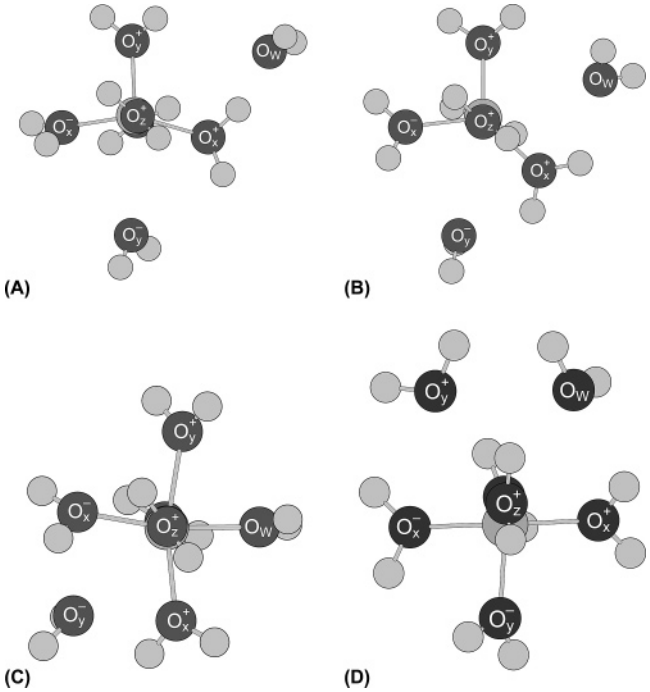

Figure 21. $Al(H_2O)_6^{3+} + H_2O$ structures from MD simulations, all with $d(Al-O_W')$ fixed at 3.0 Å. (A−C) Steps in the exchange between second-sphere water and a trans first-sphere water (A) before exchange, (B) when $d(Al-O_W') = d(Al-O_W)$, (C) after exchange; (D) $d(Al-O_W') = d(Al-O_W)$ structure in a cis exchange.

midpoint structure (Figure 21D) resembles the I_d transition state seen previously for V^{2+} and Fe^{2+}[16], as well as the I_a transition state seen for Cr^{3+}[17]; the trans midpoint resembles the I_a transition states of Mn^{3+} and Cr^{2+}[17] seen previously, as well as higher order I_a saddle points for V^{2+} and Cr^{3+}[16].

A large majority of the water exchanges seen in our MD simulations were of the trans type. Figure 20B shows the number cis exchanges as a fraction of the total number of exchanges, as a function of the Al−O_W' distance. The cis fraction initially increases with $d(Al-O_W')$, with an apparent peak near 3.0 Å (possibly corresponding to x_0), then decreases again as the total exchange fraction nears 100%. The cis fraction is never greater than 4%; in absolute terms, 49 cis exchanges out of 1376 total exchanges, out of 2000 simulations with $d(Al-O_W') = 3.0$ Å.

3.4.1. Discussion: cis versus trans Dissociative Exchange for Al^{3+}. The fact that the trans exchange is the dominant mechanism of water exchange in the MD simulations runs counter to previous experience. Kowall et al.[18] have identified the O_y^+ exchange, that is, the cis exchange, as the mechanism for water exchange in $Al(H_2O)_6^{3+}$, with a transition-state energy in good agreement with the experimental results of Hugi-Cleary et al.[21] In our own simulations, we found the cis exchange to have a lower energy barrier than the trans (*P*2 O_y^- bond angle mechanism), with 84.3 kJ/mol versus 89.7 kJ/mol; so based on this criteria, the cis exchange should be favored over the trans.

The energy barrier of a D exchange process, however, and the energy barrier of the equivalent I_d exchange may not be equal. Because of the extra negative frequency of the ab initio trans exchange maximum, we know that it should be treated as exchange barrier energy only cautiously. The I_d trans transition state, with only one negative frequency, may well be lower in energy than, and thus favored dynamically over, the I_d cis transition state. Although Al^{3+} is known experimentally to have an I_d exchange,[21] an I_d mechanism has never been produced for it by ab initio simulations.[18] Our current results

may suggest that although a cis exchanged is favored in the D process a trans exchange is favored for the I_d process.

In our MD simulations, the Al−O distance of the outgoing water was fixed so that the outgoing water did not have the option to move back into the first sphere. Therefore, what the low fraction of cis exchanges seen shows is that the trans mechanism dominates when the exchange reaction is forced to go forward. If the transmission coefficient of the cis mechanism is much higher than that of the trans mechanism, then cis could still be the dominant exchange mechanism.

4. Conclusions

We thoroughly examined the processes of first coordination sphere water dissociation and exchange in $Al(H_2O)_6^{3+}$ with various models in ab initio and molecular dynamics simulations. Using a model cluster of $Al(H_2O)_6^{3+}$ with one second-sphere water, as in previous simulations,[16−18] a dissociative (D) mechanism where the second-sphere spectator water can exchange with an outgoing water cis to it was found, having a transition-state energy of 84.3 kJ/mol, in good agreement with previous experimental[21] and theoretical[18] results.

However, the $Al(H_2O)_6^{3+} + H_2O$ cluster admits several other pathways for dissociation of a first-sphere water with a wide range of transition-state energies (63 to 91 kJ/mol) because of the symmetry-breaking role of the spectator water. The principle of microscopic reversibility, imposing the criterion that either the reaction intermediate (for D processes) or transition state (for I_d processes) for an exchange process must be symmetric with respect to the incoming and outgoing water, is necessary to distinguish which of these dissociation pathways leads to an exchange because several of them have transition states lower than the actual exchange mechanism. There is no clear relation between the wide range of transition state/intermediate energies and geometries, except that second-sphere waters hydrogen bonded to two first-sphere waters (double H-bonded) have shorter Al−O distances than second-sphere waters hydrogen bonded to only one first-sphere water (single H-bonded), with lower cluster energies. Water molecules at 300 K in molecular dynamics simulations move too energetically to form double hydrogen bonds.

A similar cis exchange mechanism was found in a model with $Al(H_2O)_6^{3+}$ and six second-sphere waters, with a transition-state energy of 81.2 kJ/mol. Additional dissociation pathways were again present, in this case as a result of rearrangements in the second coordination sphere. The hydrogen-bonding network in the second coordination sphere was sufficiently stiff that one second-sphere water was ejected to the third coordination sphere as the first-sphere water dissociated. For models with 12 second-sphere waters, the network was too stiff to allow a dissociating first-sphere water to enter, and no dissociation or exchange path was found. With multiple waters in the second coordination sphere, a dynamic second sphere is necessary to allow formation of a hole for the outgoing first-sphere water to occupy, as in molecular dynamics simulations.

A second potential D exchange mechanism was found in the $Al(H_2O)_6^{3+} + H_2O$ system, involving dissociation of a first-sphere water trans to the second-sphere water, as an O−Al−O bond angle opens to draw in the second-sphere water. This mechanism has an energy barrier of 89.7 kJ/mol but is actually a higher order saddle point with two negative frequencies, and thus not a transition state. However, a very similar I_d trans exchange mechanism occurs in the molecular dynamics simulations and makes up the vast majority of exchanges observed. (A small minority consist of cis I_d exchanges.) With the addition of a full, dynamic second coordination sphere, the extraneous negative frequency disappears and the D high-order saddle point becomes an I_d transition state. A dynamic calculation of transmission coefficients for cis and trans I_d mechanisms is necessary to determine which is actually the dominant exchange pathway in solution.

This project was motivated by the need of geochemists for a rigorous examination of ab initio methods of identifying reaction pathways. Through this analysis, we show that uncritical application to geochemical problems is dangerous. The results are strongly affected by details of the molecular cluster, and similarity of the calculated barrier energy to an experimental value alone is not sufficiently convincing evidence that the correct pathway has been identified. More convincing are molecular dynamics methods, particularly if coupled to experiments at the same scale. Although ab initio methods can identify possible pathways and calculate their energy barriers, molecular dynamics methods are needed to determine how these pathways are actually relevant to the dynamic reaction under investigation.

Acknowledgment. Support for this research was from the National Science Foundation via grant EAR 05015600 and from the U.S. Department of Energy grant no. DE-FG03-02ER15325.

Supporting Information Available: Tables summarizing key $Al(H_2O)_6^{3+} + nH_2O$ clusters. This material is available free of charge via the Internet at http://pubs.acs.org.

References and Notes

(1) Gibbs, G. V. *Am. Mineral.* **1982**, *67*, 421.
(2) Casey, W. H.; Lasaga, A. C.; Gibbs, G. V. *Geochim. Cosmochim. Acta* **1990**, *54*, 3369.
(3) Criscenti, L. J.; Kubicki, J. D.; Brantley, S. L. *J. Phys. Chem A* **2006**, *110*, 198.
(4) Criscenti, L. J.; Brantley, S. L.; Mueller, K. T.; Tsomaia, N.; Kubicki, J. D. *Geochim. Cosmochim. Acta* **2005**, *69*, 2205.
(5) Felipe, M. A.; Xiao, Y.; Kubicki, J. D. *Rev. Mineral. Geochem.* **2001**, *42*, 485.
(6) Kubicki, J. D.; Blake, G. A.; Apitz, S. E. *Am. Mineral.* **1996**, *81*, 789.
(7) Kubicki, J. D.; Xiao, Y.; Lasaga, A. C. *Geochim. Cosmochim. Acta* **1993**, *57*, 3847.
(8) Lasaga, A. C. *Rev. Mineral.* **1995**, *31*, 23.
(9) Lasaga, A. C.; Gibbs, G. V. *Am. J. Sci.* **1990**, *290*, 263.
(10) Lasaga, A. C.; Gibbs, G. V. *Geophys. Res. Lett.* **1991**, *18*, 1217.
(11) Liu, Y.; Olsen, A. A.; Rimstidt, J. D. *Am. Mineral.* **2006**, *91*, 455.
(12) Pelmenschikov, A.; Strandh, H.; Pettersson, L. G. M.; Leszczynski, J. *J. Phys. Chem. B* **2000**, *104*, 5779.
(13) Xiao, Y.; Lasaga, A. C. *Geochim. Cosmochim. Acta* **1994**, *58*, 5379.
(14) Xiao, Y.; Lasaga, A. C. *Geochim. Cosmochim. Acta* **1996**, *60*, 2283.
(15) Lee, M. A.; Winter, N. W.; Casey, W. H. *J. Phys. Chem.* **1994**, *98*, 8641.
(16) Rotzinger, F. P. *J. Am. Chem. Soc.* **1996**, *118*, 6760.
(17) Rotzinger, F. P. *J. Am. Chem. Soc.* **1997**, *119*, 5230.
(18) Kowall, T.; Caravan, P.; Bourgeois, H.; Helm, L.; Rotzinger, F. P.; Merbach, A. E. *J. Am. Chem. Soc.* **1998**, *120*, 6569.
(19) Phillips, B. L.; Tossell, J. A.; Casey, W. H. *Environ. Sci. Technol.* **1998**, *32*, 2865.
(20) Stack, A. G.; Rustad, J. R.; Casey, W. H. *J. Phys. Chem. B* **2005**, *109*, 23771.
(21) Hanauer, H.; Puchta, R.; Clark, T.; van Eldik, R. *Inorg. Chem.* **2007**, *46*, 1112.
(22) Hugi-Cleary, D.; Helm, L.; Merbach, A. E. *Helv. Chim. Acta* **1985**, *68*, 545.
(23) Phillips, B. L.; Casey, W. H.; Crawford, S. N. *Geochim. Cosmochim. Acta* **1997**, *61*, 3041.
(24) Swaddle, T. W.; Rosenqvist, J.; Yu, P.; Bylaska, E.; Phillips, B. L.; Casey, W. H. *Science* **2005**, *308*, 1450.
(25) Frisch, M. J.; Trucks, G. W.; Schlegel, H. B.; Scuseria, G. E.; Robb, M. A.; Cheeseman, J. R.; Montgomery, J. A., Jr.; Vreven, T.; Kudin, K. N.; Burant, J. C.; Millam, J. M.; Iyengar, S. S.; Tomasi, J.; Barone, V.; Mennucci, B.; Cossi, M.; Scalmani, G.; Rega, N.; Petersson, G. A.; Nakatsuji, H.; Hada, M.; Ehara, M.; Toyota, K.; Fukuda, R.; Hasegawa, J.; Ishida, M.; Nakajima, T.; Honda, Y.; Kitao, O.; Nakai, H.; Klene, M.; Li, X.; Knox, J. E.; Hratchian, H. P.; Cross, J. B.; Bakken, V.; Adamo, C.;

Jaramillo, J.; Gomperts, R.; Stratmann, R. E.; Yazyev, O.; Austin, A. J.; Cammi, R.; Pomelli, C.; Ochterski, J. W.; Ayala, P. Y.; Morokuma, K.; Voth, G. A.; Salvador, P.; Dannenberg, J. J.; Zakrzewski, V. G.; Dapprich, S.; Daniels, A. D.; Strain, M. C.; Farkas, O.; Malick, D. K.; Rabuck, A. D.; Raghavachari, K.; Foresman, J. B.; Ortiz, J. V.; Cui, Q.; Baboul, A. G.; Clifford, S.; Cioslowski, J.; Stefanov, B. B.; Liu, G.; Liashenko, A.; Piskorz, P.; Komaromi, I.; Martin, R. L.; Fox, D. J.; Keith, T.; Al-Laham, M. A.; Peng, C. Y.; Nanayakkara, A.; Challacombe, M.; Gill, P. M. W.; Johnson, B.; Chen, W.; Wong, M. W.; Gonzalez, C.; Pople, J. A. *Gaussian 03*, revision C.02; Gaussian, Inc.: Wallingford, CT, 2004.

(26) Rotzinger, F. P. *J. Chem Phys. A* **1999**, *103*, 9345.

(27) Rotzinger, F. P. *Helv. Chim. Acta* **2000**, *83*, 3006.

(28) Rotzinger, F. P. *Chem. Rev.* **2005**, *105*, 2003.

(29) Wasserman, E.; Rustad, J. R.; Xantheas, S. S. *J. Chem. Phys.* **1997**, *106*, 9769.

(30) Van Der Spoel, D.; Lindahl, E.; Hess, B.; Groenhof, G.; Mark, A. E.; Berendsen, H. J. C. *J. Comput. Chem.* **2005**, *26*, 1701.

(31) Cygan, R. T.; Liang, J.-J.; Kalinichev, A. G. *J. Phys. Chem. B* **2004**, *108*, 1255.

(32) Bock, C. W.; Markham, G. D.; Katz, A. K.; Glusker, J. P. *Inorg. Chem.* **2003**, *42*, 1538.

(33) See discussion in Casey, W. H.; Swaddle, T. W. *Rev. Geophys.* **2003**, *41*, 4/1.

(34) Bock, C. W.; Markham, G. D.; Katz, A. K.; Glusker, J. P. *Theor. Chem. Acc.* **2006**, *115*, 100.

(35) Markham, G. D.; Glusker, J. P.; Bock, C. W. *J. Phys. Chem. B* **2002**, *106*, 5118.

(36) Wang, J.; Rustad, J. R.; Casey, W. H. *Inorg. Chem.* **2007**, *46*, 2962.

(37) Bylaska, E. J.; Vallev, M.; Rustad, J. R.; Wearem, J. H. *J. Chem. Phys.* **2007**, *126*, 104505.

(38) Rustad, J. R.; Stack, A. G. *J. Am. Chem. Soc.* **2006**, *128*, 14778.

(39) Spångberg, D.; Rey, R.; Hynes, J. T.; Hermansson, K. *J. Phys. Chem. B* **2003**, *107*, 4470.